



Supplementary Materials for **Taurine deficiency as a driver of aging**

Parminder Singh *et al.*

Corresponding author: Vijay K. Yadav, vky2101@cumc.columbia.edu

Science **380**, eabn9257 (2023)
DOI: 10.1126/science.abn9257

The PDF file includes:

Materials and Methods
Figs. S1 to S7
Table S1
References

Other Supplementary Material for this manuscript includes the following:

MDAR Reproducibility Checklist

Materials and Methods

Mouse studies ethics statement

All mouse work was conducted according to International Guidelines and was approved by the Ethical Committee of the National Institute of Immunology, New Delhi, India (IAEC/AQ/2015/137) and Columbia University, New York, USA (Animal protocol # AABO2550). *C57Bl/6J* (Strain #:000664) mice were obtained from inbred wild-type colonies maintained at the National Institute of Immunology Research Support Facility or from The Jackson Laboratory. *Slc6a6*-/- mice were obtained from the Mutant Mouse Resource & Research Centers (MMRRC:044007-UCD) and are on pure *C57Bl/6N* genetic background.

10

Experimental regimens:

Lifespan analysis in mice

C57Bl/6J male and female mice were mated. They were monitored regularly for infectious agents, including pinworm and known viruses. All such tests were negative throughout the study. Each test site enrolled approximately equal numbers of 19- to 21-day-old weanlings each month over a 6-month period, housing 5 males or 5 females per cage. We used diets based on the NIH standard for breeding cages, as claimed by the manufacturer. The period between weaning and the initiation of experimental diets is given below. For breeding cages, we used Teklad Irradiated 18% protein and 6% fat diet-2918. Weanlings were put on Teklad Irradiated 18% protein and 6% fat diet-2918. This diet contains <0.3% taurine, which equals to 3–6 mg taurine consumption per mouse per day based on the average food consumption of 4–5 g per day, depending on age.

Selection of dose and frequency of taurine administration in mice. A pilot study was performed to select the suitable dose and frequency of taurine administration. This analysis showed that a single oral administration of taurine at 1000 mg per kg body weight (T1000) in middle-aged WT mice increased the peak taurine concentrations to the levels seen at baseline in young (4-week-old) WT mice (**fig. S1A**). Furthermore, taurine administration at T1000 dose daily at 10:00 am for 6 weeks increased bone structure and formation parameters (parameters that consistently decline during aging), and activated downstream targets of taurine in bone (81) [i.e., increase in extracellular signal-regulated kinase (ERK) phosphorylation and cyclin d1 (Ccnd1) levels measured using western blotting] (**fig. S1, B to D**). We note here that taurine doses used in the present study might not be optimal for all organ functions.

Mice were gavage-fed with vehicle or taurine (1000 mg per kg body weight) daily from 14 month and the treatment continued till the end of their life. Taurine was obtained from Sigma-Aldrich (T8691) and was dissolved in water for oral administration. Oral gavage was performed following standard procedures by VKY, PS, and KG who have more than 23-, 5-, and 8-years' experience, respectively, in performing this technique in various animal models (81, 89-91). A feeding needle appropriate for the age of the mouse was used. A curved gavage needle was used to reduce the likelihood of trauma in the upper gastrointestinal tract. During the procedure, mouse was held firmly, pulling up the loose skin so that it could not move its head. The head was held in vertical alignment with the esophagus. Needle tip was inserted behind the incisors and directed toward the back of the throat. During the procedure, the color of the mucous membranes was closely monitored. Vehicle or taurine solution was injected slowly, and when injection was completed, the needle was pulled out. For consistency, rigor, and reproducibility, mice were always gavaged at the same time of the day (10:00 am), all animals were fed the same normal chow, and the investigator(s) performing the body weight measurements and general health of animals were blinded to the treatment group of the mice.

Removal of mice from the longevity population

The study population for females, distributed almost equally between the two groups, consisted of 125 mice, of which 63 were assigned to the control group and 62 to the treatment group (T1000 group); three mice were removed from the study because of fighting. The study population for males, distributed almost equally between the two groups, consisted of 126 mice, of which 65 were assigned to the control group and 61 to the treatment group (T1000 group); two mice were removed from the study because of fighting. For survival analysis, mice were treated as alive at the date of their removal from the protocol, and lost to follow-up, thereafter. These censored mice were not included in calculations of median longevity.

Estimation of age at death (lifespan)

Mice were examined for signs of ill health at least once daily at 10:00 am at the time of gavage feeding in a ventilated workstation, and were killed for humane reasons if severely moribund and considered unlikely to survive for more than an additional 48 h by an experienced investigator or technician. A mouse was considered severely moribund if it showed more than one of the following clinical signs: (1) inability to eat or drink; (2) severe lethargy, as indicated by a lack of response, such as a reluctance to move when gently prodded with a pair of forceps; (3) severe balance or gait disturbance; (4) rapid weight loss over a period of 1 week or more; or (5) a severely ulcerated or bleeding tumor. The age at which a moribund mouse was killed was taken as the best available estimate of its natural lifespan. Mice found dead were also noted at daily inspections. Bodies were fixed for later necropsy analysis. For statistical analyses of survivability, the OASIS software (<http://sbi.postech.ac.kr/oasis>) was used and *p*-values were calculated using a log rank (the Mantel–Cox method) test.

Lifespan analysis in worms

***Caenorhabditis elegans* strains and maintenance**

N2 Bristol (wild-type) strain was obtained from the Caenorhabditis Genetics Center, University of Minnesota, USA and maintained at 20 °C. The strain was grown on Nematode Growth Medium (NGM) agar plates containing *Escherichia coli* OP50 bacterial lawn. All experiments were conducted with L1 synchronized worms.

Bacterial growth

Glycerol stock of the *E. coli* OP50 was streaked on Luria–Bertani plates and incubated overnight (14–16 h) at 37 °C. A single colony was inoculated in Luria–Bertani broth and grown overnight (12 h) at 37 °C for primary culture. The secondary cultures were inoculated with 1/100th volume of the primary culture and incubated at 37 °C until the optical density (OD₆₀₀) reached 0.6. The secondary cultures were concentrated 10 times and supplemented with different concentrations of taurine (0, 10, 50, 100, 150, and 300 µM). Taurine-supplemented cultures were seeded on NGM plates (250 µl for 60 mm plates). After seeding, the plates were dried, and the bacterial lawn was grown overnight before worms were placed on them.

Lifespan analysis

Wild-type worms, grown on *E. coli* OP50, were bleached and the eggs were subjected to L1 synchronization in 1X M9 for 16–18 h at 20 °C. L1 larvae were centrifuged at 2500 rpm for 1 min, the buffer was aspirated, and the larvae were placed on *E. coli* OP50 plates. Upon reaching the late L4 stage, the worms were transferred to *E. coli* OP50 plates supplemented with taurine (0, 10, 50, 100, 150, and 300 µM). The plates were overlaid with 5-fluorodeoxyuridine (FUDR, final concentration 0.1 mg per ml of medium). Lifespan scoring was started on the 7th day of adulthood and continued every alternate day. For statistical analyses of survivability, the OASIS software (<http://sbi.postech.ac.kr/oasis>) was used and *p*-values were calculated using a log rank (the Mantel–Cox method) test.

The treatment dose in worms may appear much higher compared to doses used in other species. However, there are salient differences in studies done in worms compared to oral feeding in other species where entire dose is delivered to the animal. First, the dose is mixed with live bacteria that take up the molecule, which is then layered on top of agar plates from where worms consume taurine. In addition, the bioavailability may further be reduced during the course of experiment as taurine may leach into agar, and, hence, is less available on the surface where worms reside. Moreover, worms eat more vigorously during the larval stage and their feeding declines with age due to reduction in the gut peristalsis. Besides these causes, it is possible, although it has never been tested, that the worm homolog of taurine transporter is less efficient, and thus, an initial bolus dose is required for the cellular content to reach sufficient levels.

Replicative lifespan and growth rate analysis in yeast

Yeast strains and culture conditions

All yeast strains used were in the BY4742 genetic background (MAT α his3Δ1 leu2Δ0 lys2Δ0 ura3Δ0) and have been previously described (92). For overnight culture and growth analysis, YPD (1% w/v BactoTM yeast extract (BD), 2% w/v BactoTM peptone (BD), 2% w/v dextrose) medium was used. Yeast were cultured at 30 °C for all experiments.

A modified RLS protocol for treatment was developed based on previously described methods (93, 94). Briefly, cells were grown on freshly prepared YPD plates at 30 °C until single colonies were visible. Cells were selected from a single colony and lightly patched onto YPD plates and incubated at 30 °C for 24 h. For experiments performed on YPD medium, cells were lightly patched onto fresh YPD plates supplemented with 0 μM, 1 μM, 10 μM, 100 μM, 300 μM, 1 mM, or 100 mM taurine and allowed to grow overnight. For experiments performed on synthetic complete (SC) medium, cells were lightly patched onto SC plates (0.05% w/v ammonium sulphate, 0.2% w/v Synthetic Complete Hopkins Mixture, 0.17% w/v Yeast Nitrogen Base without amino acids, 2% w/v Bacto Agar, 2% w/v dextrose) supplemented with 0 μM, 1 μM, 10 μM, 100 μM, 300 μM, 1 mM, and 100 mM taurine. In both cases (YPD and SC experiments), in the morning founder cells were aligned and selected as newborn daughter cells using a micromanipulator. Cells were monitored for cell divisions every 90–120 minutes, and budded daughter cells were separated and removed as they formed. The process continued until cells stopped dividing. Replicative lifespan was calculated as the number of times each mother cell divided before it underwent permanent cell cycle arrest. Plates were kept overnight in a refrigerator at 4 °C. Plates were kept wrapped in tinfoil except while being dissected to avoid potential light sensitivity of any compound. All experimenters were blinded to the identity of any of the treatments at the time of dissection. Cells were dissected in groups of 20.

Analysis of growth rate in yeast strains was performed using a Bioscreen C MBR (Growth curves USA, Piscataway NJ, USA) as previously described (95). Raw optical density data were smoothed using the R package “smooth.spline,” as previously described (96). Doubling times were calculated using the inflection method—identifying the maximum semi-log slope along growth curves within the optical density range linearly correlated with number of yeast cells—with the online web tool Yeast Outgrowth Data Analyzer (YODA) (97). All experiments were repeated with at least three biological replicates.

Phylogenetic analysis of taurine biosynthesis across evolutionary landscape

The CSAD ortholog/paralog information for the selected species (human, monkey, mouse, rat, chicken, xenopus, zebrafish, drosophila, *C. elegans*, and yeast (Baker’s)) was obtained from KEGG (https://www.kegg.jp/kegg-bin/view_ortholog_table?map=00430), and the protein sequences in the FASTA format, based on the KEGG IDs, were obtained from UniProt DB. The

sequences were aligned with Multiple Sequence Comparison by Log-Expectation (MUSCLE) using the MEGA11 software. A best model was obtained using the Maximum likelihood (ML) method with the MEGA11 software. The LG+G matrix was used to construct the tree.

5 **Healthspan analysis in middle-aged mice treated with vehicle or taurine**

Oral gavage of taurine or vehicle in mice

Effect of taurine in aged mice was investigated using 14-month-old *C57Bl/6J* female and male mice (RRID: IMSR_JAX:000664). Mice were gavage-fed with vehicle or taurine (500 or 1000 mg per kg body weight) daily for 10–12 month and culled at the age of 24 months for terminal assays. For consistency, rigor, and reproducibility, mice were always gavaged at the same time of the day (10:00 am), each physiological assay was performed at the same time of the day (indicated separately for each assay), all animals were fed the same normal chow, and the investigator(s) performing the measurements were blinded to the genotype or treatment of mice.

In-life procedures and assays in mice

15 In-life assays were performed for the assessment of healthspan, as described below. A schematic diagram of the order of tests performed in mice is presented in **fig. S2A and S3A**. The following main tests were performed in live mice: glucose tolerance test, insulin tolerance test, grip strength test, rotarod test, wire hanging test, light-dark test, energy expenditure measurement tests, Y maze test, gastrointestinal transit test, and immunophenotyping test. Detailed protocols for each of these tests and the order in which they were performed to maximize the information obtained per mouse without compromising the rigor of the study are presented below. We should mention here that these tests are routinely performed in consultant laboratories, Columbia University Core facilities with extensive expertise in various organ functions.

Rotarod test

25 Motor coordination and imbalance were tested (between 11:00 am–13:00 pm) using a rotarod apparatus (model 7650 Rota-rod, UgoBasile, Collegeville, PA, USA), as described previously (90, 98). The apparatus consists of a plastic rod (diameter, 6 cm) and five equal sections separated by six disks (diameter, 25 cm), which allows five mice to be tested simultaneously. Before the test day, mice were trained on the rotarod apparatus for 3 consecutive days. On the testing day, mice were acclimated to the environment for 30 min. They were then placed on the rotating rod, which had a speed of 10 or 30 rpm. The maximum duration of each trial was set to 5 min. When the mice fell off the rod, the time was recorded. There were 5 min breaks between each recording speed. The mean latency to fall off the apparatus was used as a performance value (98).

Grip strength measurement

35 The grip strength test was used to measure the neuromuscular function as maximal muscle strength of forelimbs at 10:00 am (90). The test was assessed based on the grasping of the mouse on a grid that was connected to a sensor, as described previously (90). Three trials were carried out in succession to measure the forelimb-strength only, followed by three successive trials to measure the combined forelimb/hindlimb grip strength. All grip strength values obtained were normalized against the mouse body weight.

Y-maze test for memory

45 Y-maze tests were performed as described previously (90). The maze had a diameter of 150 cm and contained water (23 °C), made opaque with non-toxic white paint. The pool was located in a brightly lit room with distal visual cues, including computer, tables, and posters with geometric figures attached to the walls. Mice were transported to the testing room in their home cages filled with wooden bedding and left there undisturbed for at least 30 min. Spatial learning was assessed across repeated trials (4 trials per day for 10 days). During trials, a small platform (diameter, 10 cm) was hidden beneath the surface at a fixed position. A round platform (diameter, 15 cm) was

hidden 1 cm beneath the water surface at a fixed position. Each daily trial block consisted of four swimming trials (15 min, inter-trial interval), starting randomly from each of the four starting positions. Mice that failed to find the platform within 2 min were guided to the platform. They had to remain on the platform for 15 s before they were returned to their cages. Mice were placed in water at the border of the maze and had to reach the platform after which they were transported back to their home cage. Mice that did not reach the platform within 2 min were gently guided toward the platform and were left on it for 10 s before being placed back in their cages. Four of such daily training trials (intertrial interval, 5 min) were given on 10 subsequent days. Starting positions in the pool varied between four fixed positions (0°, 90°, 180°, and 270°). Because a decrease in latency to find the platform was already present on the second acquisition day, the first acquisition day is also reported.

Food intake measurement

Food intake was measured using metabolic cages. Briefly, mice were individually housed in metabolic cages (Nalgene, Rochester, NY) and fed ad libitum. Amount of food consumed was determined by weighing the powdered chow before and after the 24-hour period in the metabolic cages.

Gastrointestinal transit test

Gastrointestinal transit tests in mice were performed at 12:00 pm, as described previously (99).

Tail suspension test

The tail suspension test was conducted at 12:00 pm, as previously described (42, 100). Mice were securely fastened by the distal end of the tail to a flat metallic surface and suspended in a visually isolated area (40 × 40 × 40 cm white Plexiglas box). The presence or absence of immobility, defined as the absence of limb movement, was assessed every 5 s over a 6 min test session by a highly trained observer who remained blind to the genotype.

Glucose and insulin tolerance tests

For GTT, glucose (2 g per kg body weight) was injected intraperitoneally (i.p.) after an overnight (16 h) fast, and blood glucose was monitored using blood glucose strips and the Accu-Check glucometer (Roche) at indicated times. For ITT, mice were fasted for 6 h, injected i.p. with insulin (0.2 U per kg body weight), and blood glucose levels were measured at indicated times as described previously (101). The ITT data are presented as percentages of initial blood glucose concentration. For both GTT and ITT, area under the curve was calculated, as described previously (101).

Indirect calorimetry

Metabolic assessments were performed at room temperature (23°C) with a 12:12 h light/dark cycle in the room (lights on 7:00 am, lights off 07:00 pm) for 2 consecutive days. The indirect calorimetry trial was conducted in metabolic cages equipped with water bottles. Mice were placed individually into these metabolic cages for about 4 h before the actual recordings were started. Mice were granted free access to food and water. Metabolic cages were set up in a quiet behavioral assessment room and were continuously supplied with fresh air. Variations in O₂ and CO₂ levels were recorded by high precision O₂ and CO₂ sensors in each individual cage. Combined with parallel airflow measurements, this enabled calculation of oxygen consumption (expressed as ml O₂ per hour per animal) over a given time period. The system also monitored CO₂ production, and, hence, it was possible to determine the respiratory exchange ratio (RER) and heat production (HP). The RER was calculated as the VCO₂/VO₂ ratio. Heat production (Kcal per hour) was measured and normalized to body weight of each mouse. In addition, body mass was recorded before and after gas exchange measurements. Physical activity was monitored using infrared light beams set-up, within the metabolic cages.

Terminal analysis

Mice were culled at the indicated time points and tissues were processed for various assays to assess parameters that cannot be assessed non-invasively or require collection of blood volumes that have the potential to affect in-life assays. Following terminal assays were performed in mice (n = 10, for each sex and genotype).

Bone histology and histomorphometry

Skeletal processing and histological and histomorphometric analyses were performed, as described previously (81). For histological analysis, mice were euthanized at indicated ages between 11:00 am and 02:00 pm. Briefly, for assessment of dynamic histomorphometric indices, mice were injected with calcein, 2 and 4 days prior to sacrifice, according to the standard calcein double-labeling procedure (81). After sacrifice, internal organs were removed from the animals and whole skeleton was pinned to a thermocol board and immersed in 4% neutral buffered formalin for 12–14 h at room temperature. After fixation, the skeleton was cut into vertebral column (Lumbar vertebra 1 to 5, with associated muscles) or long bone (with associated muscles) for processing and embedding. Undecalcified bones were dehydrated in a graded series of ethanol, embedded in methyl methacrylate, and 5 µm sections were prepared on a rotary microtome (Leica Inc.), as described previously (81). Sections were stained with 1% toluidine blue (osteoblast parameters), Von Kossa/Van Gieson reagent (stains mineralized bone matrix in black and non-mineralized bone matrix in red), or tartrate-resistant alkaline phosphatase (TRAP, osteoclast parameters) stain and visualized under a Zeiss microscope (Carl Zeiss, Jena, Germany). Histomorphometric analysis was performed on tibiae and vertebrae according to the American Society for Bone and Mineral Research (ASBMR) standards (102) using the OsteoMeasure Analysis System (OsteoMetrix, Atlanta, GA). For BV over total volume % (BV/TV%) analysis, Von Kossa/Van Gieson-stained sections were imaged at 5× magnification and analyzed using the Image J software. For osteoblast parameters, toluidine blue-stained sections were visualized at 20× magnification and analyses were performed in the secondary spongiosa in at least 15 fields per vertebra or long bone section. For osteoclast parameters, TRAP-stained sections were visualized at 20× magnification and analyses were performed in the secondary spongiosa in at least 15 fields per vertebra or long bone section. For bone formation analysis, sections were cleared in xylene, mounted in DPX, and visualized under ultraviolet light at 40× magnification, and analysis was performed to detect bone formation fronts.

Micro-computed tomography (μ CT) analysis

Trabecular bone and cortical architecture of the proximal tibia were assessed using a μ CT system (Skyscan 1172), as described previously (90, 103). Tibia bone specimen was stabilized with gauze in a 2 ml centrifuge tube filled with 70% ethanol and fastened in the specimen holder of the μ CT scanner. One-hundred μ CT slices, corresponding to a 1.05 mm region distal from the growth plate, were acquired at an isotropic spatial resolution of 10.5 µm. A global thresholding technique was applied to binarize grayscale μ CT images where the minimum between the bone and bone marrow peaks in the voxel gray value histogram was chosen as the threshold value. The trabecular bone compartment was segmented using a semi-automatic contouring method and subjected to a model-independent morphological analysis (104) using the standard software provided by the manufacturer of the μ CT scanner. The 3D morphological parameters, including model-independent measures by distance transformation (DT) of bone volume fraction (BV/TV), Tb.Th* (trabecular thickness), Tb.N* (trabecular number), Tb.Sp* (trabecular separation), and connectivity density (Conn.D), were evaluated. The Conn.D is a quantitative description of the trabecular connection (105, 106).

Immunotyping of the spleen and blood

Immune cell profiling of the spleen was done using flow cytometry. Spleen was dissected from mice, culled by cervical dislocation at 12:00 pm, and crushed between a pair of frosted slides to obtain a single cell suspension. Red blood cells in the suspension were lysed by osmotic shock using water; cells were then washed and resuspended in complete medium. Phenotyping of various immune cells in the mouse spleen was done using the following antibodies from BD: B220 (RA3-6B2), CD4 (RMA4-5), CD8 (53-6.7), CD25 (PC61.5), Foxp3 (FJK-16s), CD11b (M1/70), Gr-1 (RB6-8C5), and NK1.1 (12-5941-82). Staining was done by incubating 1 million cells in staining buffer (PBS containing 2% BSA and 0.05% Na₃N) for 30 min at 4 °C. The cells were washed twice with cold staining buffer and samples were acquired on BD Verse; the analysis performed using FlowJo (Treestar).

Immune cell profiling of the blood was done using a hematology analyzer. For this purpose, blood was collected from the animals in citrate phosphate dextrose (CPD) anticoagulant-containing syringe. Hematology was performed with fresh blood using a hematology analyzer MS 4e Automated Cell counter.

Generation of mouse and rat postmenopausal osteoporosis model and taurine treatment regimens

Effect of taurine on ovariectomy-induced bone loss in mice and rats

We subjected 6-week-old virgin female mice or 12-week-old virgin female rats to either bilateral ovariectomy or sham operation. Post-ovariectomy animals were left untreated for 6 weeks to develop osteopenia following established protocols (89). After this 6-weeks drug holiday period, the animals were gavage-fed vehicle or taurine (0 or 1000 mg per kg body weight per day) in distilled water daily at 10:00 am for 6 (for mice) or 12 (for rats) weeks. The animals were sacrificed at the end of the treatment period to collect skeleton and processed for bone histology and histomorphometry, as described previously (89). At the time of sacrifice, uterine weight was measured to confirm the successful removal of ovarian steroids. All ovariectomized animals, irrespective of their treatment (vehicle or taurine), showed atrophied uteri compared with sham vehicle-treated controls.

Cellular assays

Isolation and culture of primary osteoblasts

Calvarial bone was obtained from infants (2–3-days-old) for osteoblast isolation and culture, as described previously (89). Animals were culled using CO₂ and autoclaved sterile scissors and forceps were used to carefully dissect out the calvarial bone, which were immediately transferred to ice cold Hank's Balanced Salt Solution (HBSS) medium. Muscles were removed and bone fragments were washed twice with ice-cold HBSS medium to remove any contaminating blood cells. The bone fragments were taken out on sterile petri dishes in a cell culture hood and were finely chopped with a sterile scalpel. These finely chopped fragments were sequentially digested in 2 ml alpha-MEM with collagenase at a concentration of 10 mg per ml for 10–15 min on water bath at 120 rpm at 37 °C. The first supernatant was discarded and sequential digestion with collagenase containing medium was repeated four times. The supernatants from all the digestions were collected into 15 ml falcon containing FBS. These tubes containing approximately 10 ml of fragments were centrifuged at 800 rpm for 5 min at 4 °C to collect the tubules and discard the osteoblasts. Alpha-MEM was used to wash these cells twice to remove any traces of collagenase. The final tissue pellet was resuspended in 10 ml of warm alpha-MEM containing 10% FBS. The cells were seeded on a 6-well plate kept in a humidified cell culture chamber at 37 °C with 5% CO₂. Next day, the existing medium was removed and cells were gently washed with prewarmed

alpha-MEM. This was done to remove any contaminating cells that might have adhered to the osteoblast culture. The medium was changed after every 2 days. Cells were passaged after the culture was confluent, and P2 and P3 cells were used at different times for various treatments and analyses.

5 **Mineralization assay of primary osteoblasts**

Primary osteoblasts from mice were seeded in a 6-well plate at a seeding density of 1×10^6 in a differentiating medium (α -MEM with 10 mM β -glycerophosphate, 50 μ g per ml ascorbic acid and 100 nM dexamethasone). Mineralized nodules were visualized by staining the fixed cells with Alizarin red-S stain and the stain was extracted with 10% cetylpyridinium chloride to quantify mineralization colorimetrically (OD at 595 nm).

10 **Alkaline phosphatase assay of primary osteoblasts**

After 6 days of differentiation, osteoblasts were fixed in 2.5% glutaraldehyde and stained with an Acid Phosphatase staining kit (387 A, Sigma-Aldrich, St. Louis, MO, USA), according to the protocol prescribed by the manufacturer.

15 **Senescence associated beta-galactosidase staining assay on osteoblasts**

Bone marrow-derived mesenchymal stem cells were differentiated into osteoblasts, as described previously (81). On day 6 post differentiation, a 10 Gray (Gy) dose of irradiation was used for inducing senescence, as described previously (107). Following irradiation, the medium was changed and cells were cultured in the presence or absence of taurine (20 mM) for 7 days before performing the beta-galactosidase staining. Beta-galactosidase staining was performed on cells, as described previously (107).

20 **Culture of rat N27 dopaminergic neuronal cell line for viability assays**

Rat N27 dopaminergic neuronal cells were cultured in RPMI 1640 medium with 10% fetal bovine serum and 1% penicillin/streptomycin at 37 °C with 5% CO₂. The cells were cultured in T-75 flasks for passaging, and in 96-well flat bottom culture plates for the viability assay. The cell viability was quantified colorimetrically using the 3-(4,5-dimethylthiazol-2-yl)-2,5 diphenyl tetrazolium bromide (MTT) assay. The viable cells with active mitochondria reduce the colorless MTT to produce dark blue DMSO-soluble formazan crystals. For MTT assay, 5000 N27 cells at a density of 50 cells per μ l were plated in 96-well flat bottom plates and incubated for 24 h at 37 °C incubator before the treatment. After 24 h, cells were preincubated with taurine (0–5 mM concentration) for 1 h followed by cotreatment with toxins, paraquat (PQ, 500 μ M) and manganese (Mn, 500 μ M) for 48 h. Three hours before the end of the experiment, 50 μ l MTT solution (5 mg per ml) was added to each well of the 96-well plate and returned to the 37 °C incubator. After 3 h of incubation, the medium was decanted, and the formazan precipitate was solubilized in 200 μ l DMSO and incubated for 30 min in the 37 °C incubator. Color intensity was quantified at 570 nm. Each experiment was performed in three repeats, with five wells per repeat. The bar graph shows a representative experiment with percent survival \pm standard deviation relative to control. The *p*-value was calculated using one-way ANOVA with Tukey's multiple comparison test. The *p*-values are represented as *p* ≤ 0.0001****, *p* ≤ 0.001***, *p* ≤ 0.01**, and *p* ≤ 0.05*.

40 **RNA sequencing and analyses**

RNA was extracted from the mouse primary calvarial osteoblasts prepared from day 3–5 neonates of WT or *Slc6a6*−/− genotypes using the RNeasy extraction kit (Qiagen). RNA sequencing libraries were prepared with Illumina-compatible NEBNext Ultra™ II Directional RNA library kit at Genotypic Technology, Inc. The raw data were trimmed for adapter sequences and low-quality bases (<q30) using Cutadapt with default parameters and checked for quality using FastQC (<https://www.bioinformatics.babraham.ac.uk/projects/fastqc/>). Mouse raw reads were aligned to the mouse reference genome (mm9) using Hisat2 (108) with default parameters. HTSeq (109) was

used to estimate gene abundance. Downstream analyses were done using the analysis framework tidybulk (48, 110). The filterByExpr functionality of edgeR (111) was used to identify the abundant gene-transcripts included in downstream analyses using default parameters and the knock-out phenotype as the factor of interest. The algorithm trimmed mean of M valued (TMM) values identified sample-wise scaling to compensate for differences in sequencing depth across samples (112). For aiding data exploration, we reduced the data dimensionality using principal component analysis (PCA). Differential expression analyses were performed using the robust likelihood ratio implementation of edgeR, testing for difference in gene transcript abundance greater than 1 log-fold (113, 114). The ppcseq method was used to investigate the presence of outlier observation among the significant results to avoid biases in the statistics (115). The ggplot2 software produced most of the data visualizations, whereas tidyHeatmap was used for heatmap visualization (116-118).

We performed gene-set enrichment analyses using the MSigDB C2 experimentally derived gene set, the clusterProfiler algorithm, and the visualization tool enrichplot (cran.r-project.org/) (<https://rdrr.io/cran/msigdb/>) (119). An aging signature was composed of a union of gene sets from MSigDB and a set of genes derived from aging datasets identified in this study through gene set enrichment analysis and published literature (120). The *p*-values of gene set analyses were corrected for multiple testing using the Benjamini Hochberg correction (121).

Code availability

The code used for data analysis is stored publicly at [github, stemangjola/singh_et_al_taurine_bone](https://github.com/stemangjola/singh_et_al_taurine_bone).

Data availability

Scaled counts have been deposited at [10.5281/zenodo.7700452](https://zenodo.10.5281/zenodo.7700452)

Analysis of aging hallmarks in middle-aged mice, *Slc6a6*-/- mice, and in mammalian cells, following taurine treatment

Senescence-associated β-galactosidase (SA β-Gal) assay in mouse tissues

SA β-Gal assay was performed using the Senescence Detection Kit (ab65351), designed to histochemically detect the SA β-Gal activity, a known characteristic of senescent cells, in mammalian cells and tissues. The SA-β-Gal is present only in senescent cells and is not found in pre-senescent, quiescent, or immortal cells. Briefly, tissues were collected in 1× PBS and fixed in 10 volumes of fixative/tissue for 1 h at room temperature on an orbital shaker. Following fixation, tissues were washed in 1× PBS and kept on ice until all the animals were sacrificed. SA β-Gal staining was performed overnight at 37 °C. Tissues were observed under a dissecting bright field microscope (Leica Inc.) for the development of blue color (×1 magnification) and cleared in alcohol for 2–3 days before visualization except for fat. For the fat, whole mount staining tissues were washed following staining in 1× PBS and imaged directly without clearing them in alcohol.

PQ-induced toxicity in wild-type mice

Male C57BL/6J mice were purchased from The Jackson Laboratory at 8 weeks of age. Mice were randomized to receive either taurine, 1000 mg per kg per day once daily for 10 days or an equal volume of vehicle. On day 31, mice were injected with 50 mg per kg paraquat dichloride (Sigma). For survival analysis, viability was recorded every 12 h after paraquat injection and the survival curve was generated using the GraphPad5 software.

Western blot analysis

Western blot analysis was performed according to standard protocols. Briefly, 25–30 µg of total protein was separated on 10–12% SDS-PAGE gels and then transferred onto PVDF membrane (Millipore, Inc.). After blocking with 5% BSA for 1 h, membranes were incubated with specific antibodies overnight at 4 °C. Following antibodies were used: p-RS6P-Ser235/236 (1:1000;

catalog #2211; Cell Signaling Technology), RS6P (1:1000; catalog #2217; Cell Signaling Technology), Trimethyl-H3K27 (1:1000; catalog #9733; Cell Signaling Technology), Trimethyl-H3K9 (1:1000; catalog #13969; Cell Signaling Technology), Histone H3 (1:1000; catalog #4499; Cell Signaling Technology), LC3A/B (1:1000; catalog #4108; Cell Signaling Technology), PGC1 (1:1000; catalog #ab54481; Abcam), UCP1 (1:1000; catalog #ab209483; Abcam), UCP2 (1:1000; catalog #ab97931; Abcam), Total OXPHOS Rodent WB antibody cocktail (1:1000; catalog #ab110413; Abcam), ND6 (1:1000; catalog #ABIN6263413; antibodies-online.com), GTPBP3 (1:1000; catalog #ARP93298; Aviva Systems Biology), MTO1 (1:1000; catalog #15650-1-AP; Proteintech), p-ERK (1: 1000; catalog #9106; Cell Signaling Technology), ERK (1:1000; catalog #9102; Cell Signaling Technology), GAPDH (1: 20,000; catalog #sc-32233; Santa Cruz Biotechnology) and β-actin (used as loading control; 1:5,000; catalog #A5541; Sigma). After incubation with the primary antibody, membranes were washed in 1× TBST, incubated with secondary antibodies for 1 h at room temperature, and visualized using the Bio-Rad chemiluminescence reagent. Images were acquired using the Invitrogen gel documentation system.

15 **Cytokine profiling by multiplex cytokine assay**

A multiplex biometric enzyme linked immunosorbent assay (ELISA)-based immunoassay, containing dyed microspheres conjugated with a monoclonal antibody specific for a target protein, was used according to the manufacturer's instructions (23-plex Cytokine Assay; BioRad Inc., Hercules, CA). The cytokines measured were granulocyte colony stimulating factor (G-CSF), granulocyte–monocyte colony stimulating factor (GM-CSF), IFN-γ, IL1-α, IL1-β, IL2, IL4, IL5, IL6, IL7, IL9, IL10, IL12 (P40), IL12 (P70), IL13, IL15, IL17, IP10, KC, EO, CCL2 (monocyte chemoattractant protein (122)- 1), CCL4 (macrophage inflammatory protein [MIP]-1β), MIP-1α, MIP2, RANTES, and TNFα. Briefly, serum samples were diluted 1:4 and incubated with antibody-coupled beads for 2 h at room temperature with shaking. The immune complexes were washed, then incubated with biotinylated detection antibody for 1 h at room temperature, and incubated for 30 min with streptavidin–phycoerythrin prior to assessing cytokine titers. Concentrated human recombinant cytokine was provided by the vendor (BioRad, Inc.). A broad range, 1.95–32,000 pg per ml, of standards was used to establish standard curves to maximize the sensitivity and dynamic range of the assay. Cytokine levels were determined using a Bio-Plex array reader (an automated flow-based microfluidics device that uses a dual-laser fluorescent detector with real-time digital signal processing for quantitation; Luminex, Austin, TX). This instrument quantitates multiplex immunoassays in a 96-well format on very small fluid volumes. The concentrations of analytes in these assays were calculated using a standard curve with the software provided by the manufacturer.

35 **Preparation of muscle homogenates and mitochondrial ROS measurements**

Quadriceps and gastrocnemius (~50–100 mg) were cleaned of red muscles and washed in 5 ml of ice-cold PBS per 10 mM EDTA. Ligaments, fat, and connective tissue were removed by trimming the muscle, which was then minced into small pieces. Cleaned muscle tissue was then transferred to an ice-cold solution of PBS/10 mM EDTA plus 0.05% Accutase and incubated for 30 min. After centrifugation at 200 × g for 5 min at 4 °C, the pellet was resuspended in 1 ml of Hanks' balanced salt solution (HBSS) and homogenized with a glass homogenizer (10 to 15 strokes, 400 rpm). The protein content was normalized to 2 mg per ml in HBSS, and 200 µl of the solution was transferred to 1.5 ml black Eppendorf tubes. Mitochondrial ROS levels were assessed using the fluorescent dye, Red Mitochondrial Superoxide Indicator (MitoSOX; final concentration, 5 µM). After 45 min incubation at 37 °C, muscle homogenate was centrifuged at 500 × g for 3 min and washed with 250 µl of HBSS. The centrifugation and washing steps were repeated twice. Finally, the pellet was resuspended in 200 µl of HBSS, and 100 µl of the preparation was transferred to a black 96-well

plate (in duplicates). MitoSOX triggers the formation of red fluorescent products that were detected at 531 nm (excitation)/595 nm (emission). The intensity of fluorescence is proportional to mitochondrial ROS levels. The fluorescence was measured using a BioTek fluorimeter.

Measurement of serum 8-OH-dG levels in mice and monkeys.

A DNA damage ELISA kit (Invitrogen Cat # EIANAD) was used to measure changes in 8-OH-dG levels in liver or serum samples according to manufacturer's instructions. Serum samples were diluted 1:8 in the assay buffer before measurement.

Lipid peroxidation

Lipid peroxidation was measured in extracts of liver or in serum (monkeys) using a Lipid Peroxidation (MDA) Assay kit (Abcam) according to the manufacturer's protocol. The liver tissue (15–20 mg) was homogenized in lysis solution, and the protein concentration was determined by measuring OD260. The malondialdehyde (MDA) concentrations were measured on a microplate at 532 nm using a BioRad plate reader. MDA concentrations were normalized to the protein content to calculate the absolute levels of lipid peroxidation.

Measurement of protein carbonyls

Concentrations of protein carbonyls were assessed in heart protein extracts using the Protein Carbonyl ELISA Kit (Abcam) according to the manufacturer's instructions. In brief, protein samples were adjusted to 10 µg/mL and allowed to adhere overnight at 4 °C to wells of a 96-well plate provided by the manufacturer. Subsequently, reaction with dinitrophenylhydrazine (DNPH) was performed for derivatization of the protein carbonyl groups. The DNP-modified proteins were probed with anti-DNP antibody and developed with secondary HRP-conjugated antibody. Following substrate addition, absorbance (OD450) was measured with a BioRad multifunctional plate reader and carbonyl content in protein samples was determined by comparing its absorbance with that of a known reduced/oxidized bovine serum albumin standard curve. Each sample was measured in duplicate.

DNA methylation and clustering analysis

DNA Extraction: DNA was extracted using the Quick-DNA Magbead Plus Kit (Cat#: D4082), following the manufacturer's instructions. Library Preparation: The EZ DNA Methylation-Lightning Kit (Zymo Research, Irvine, CA) was used for bisulfite conversion, following the standard protocol. Samples were enriched specifically for the sequencing of >2000 age-associated gene loci using Simplified Whole-panel Amplification Reaction Method (SWARM®), where specific CpGs are sequenced at minimum 1000X coverage. The sequencing was performed on the Illumina NovaSeq instrument. The methylation level of each sampled cytosine was clustered using Pearson correlation method and heatmaps were generated using Pheatmap library in R (version 4.1.2). Row and column distance for clustering in all the heatmaps are based on 1-Pearson correlation with Complete linkage.

LC-MS-based analysis of tRNA modification

Total RNA was isolated from the liver tissue samples using the TRIzol method according to standard protocols. Before performing the LC-MS-based detection of tRNA modification, the integrity and quantity of each RNA sample was checked using agarose gel electrophoresis and the NanoDrop™ instrument. tRNA isolation: tRNA was isolated from total RNA samples using NEBNext Poly(A) tRNA Magnetic Isolation Module (NEB, E7490). Purified tRNA was quantified using the Qubit RNA HS Assay kit (ThermoFisher, Q32855). tRNA digestion and LC-MS analysis: tRNA was hydrolyzed to single nucleosides and then nucleosides were dephosphorylated using an enzyme mix. Pretreated nucleoside solution was deproteinized using Sartorius 10,000-Da MWCO spin filter. Analysis of nucleoside mixtures was performed on Agilent 6460 QQQ mass spectrometer with an Agilent 1260 HPLC system. Multi reaction

monitoring (MRM) mode was performed considering the high selectivity and sensitivity attained working with parent-to-product ion transitions. Data acquisition and analysis: LC-MS data were acquired using the Agilent Qualitative Analysis software. MRM peaks of each modified nucleoside were extracted and normalized to the quantity of purified tRNA. The results are expressed relative to controls.

RNA in situ hybridization

RNAscope assay (Advanced Cell Diagnostics, Cat. No. 323110) was performed according to manufacturer's protocol on 7 µm deparaffinized sections with probes for *Slc6a6* (ACD, Cat No. 523331-C2) and *Lgr5* at 40 °C for 1 h and revealed with Opal570. Confocal images were acquired using a laser-scanning confocal inverted microscope (LSM700, Carl Zeiss Inc.). We have not performed a comprehensive analysis of stem cell markers across tissue types and our analysis was restricted to the gut and skin. Moreover, we only assessed changes in the expression of *Lgr5*, which reportedly expresses in stem or progenitor cells of the gut and skin (61).

Analysis of the effect of taurine on telomerase deficiency-induced senescence in zebrafish (*Danio rerio*)

Ethics statement

Experiments on zebrafish were conducted according to local and international guidelines approved in France by the Animal Care Committee of the IRCAN, the regional (CIEPAL Cote d'Azur #697) and national (French Ministry of Research #27673-2020092817202619) authorities.

Zebrafish maintenance and generation of G2 tert-/-

The telomerase mutant line, *tert* AB/hu3430, is available at the ZFIN repository, ZFIN ID: ZDB-GENO-100412-50, from the Zebrafish International Resource Center (ZIRC). The G1 *tert* hu3430/hu3430 homozygous mutant was obtained by intercrossing the *tert* AB/hu3430 (*tert* +/-) strain. WT siblings were used as WT controls. The G2 *tert* -/- fish were obtained by intercrossing the G1 *tert* -/- and the WT control was obtained by intercrossing the WT siblings of the G1 *tert* -/-. Embryos were collected from crosses and kept in E3 embryo medium (5.0 mM NaCl, 0.17 mM KCl, 0.33 mM CaCl₂, 0.33 mM MgSO₄, 0.05% methylene blue, pH 7.4) at 28 °C on a 14 h light/10 h dark cycle.

Treatment of zebrafish larvae

At 2 days post-fertilization (dpf), *tert* -/- fish with severe phenotype were discarded because they were beyond rescue. The remaining fish were randomly distributed between the different treatment groups. Treatment was carried out in 12 well plates, 20 larvae per well with 3 ml of E3 alone or E3 with 300 µM or 10 mM of taurine. Embryos were visualized daily for assessment of viability. Treatment was also renewed every day and animals were fed started at 6 dpf. Embryos were collected at 5 dpf for β-Gal assay.

Senescence-associated β-galactosidase assay

Five days post-fertilization larvae were fixed overnight in 4% paraformaldehyde at 4 °C, washed three times for 1 h in PBS (pH 7.4), and for a further 1 h in PBS (pH 6.0) at 4 °C. β-Galactosidase staining was done for 10 h at 37 °C in 5 mM potassium ferrocyanide, 5 mM potassium ferricyanide, 2 mM MgCl₂, and 1 mg per ml X-gal, in PBS adjusted to pH 6.0. After staining, larvae were washed three times for 5 min in PBS (pH 7), followed by imaging using a bright filter stereoscope.

RNA extractions and qPCR

Embryos were homogenized in TRIzol and RNA was extracted using phenol-chloroform method. Quality of RNA samples was assessed through BioAnalyzer (Agilent 2100, CA, USA). Reverse-transcription into cDNA was performed using a RT-PCR kit NZY First-Strand cDNA Synthesis Kit # MB12501 (NZYtech). Quantitative PCR (qPCR) was performed using iTaq Universal SYBR

Green Supermix # 1725125 (Bio-Rad) and a StepOnePlus™ Real-Time PCR System (Life Technologies). qPCRs were carried out in triplicate for each cDNA sample. Relative mRNA expression was normalized against actin mRNA expression using the $\Delta\Delta CT$ method. Primer sequences are listed below: *tert*, F: 5'-CGGTATGACGGCCTATCACT-3'; R: 5'-TAAACGGCCTCCACAGAGTT-3'; *actb1* (actin-beta), F: 5'- GGACCTGTATGCCAACACTGTA -3'; R: 5'- ATGTGATCTCCTCTGCATCCT -3'.

Combinatorial senolytic treatment in *Slc6a6*-/- mice

Eight-month-old *Slc6a6*-/- mice were randomized to receive every alternate week vehicle or D (5 mg per kg body weight) + Q (50 mg per kg body weight) by oral gavage in 100–150 μ l 10% PEG400. Treatment was stopped after 4 months and animals were analyzed for function of various organs, 4 days after the last administration. For the lifespan assessment animals were maintained on the senolytic regimen until the end of their life.

Rapamycin treatment of *Slc6a6*-/- mice

Four-month-old *Slc6a6*-/- mice were randomized to receive vehicle or rapamycin (8 mg per kg body weight per day, i.p.) by intraperitoneal injection on the opposite sides of the belly on alternate days in 200–300 μ l. For the injection, rapamycin (LC Laboratories) was dissolved in DMSO to 100 mg per ml, and then further diluted in 5% PEG-400/5% Tween-20 to a final concentration of 1.2 mg per ml; it was filter sterilized, aliquoted, and stored at –80 °C for long-term storage. Six mice (females) were i.p. injected, daily for 1 month, 66 μ l per 10 g body weight rapamycin to achieve a final dosage of 8.0 mg per kg starting at 16-weeks of age. Control WT or *Slc6a6*-/- mice (females) were i.p. injected with vehicle solution (5% PEG-400/5% Tween-20) for 1 month. Body weight was measured at baseline and then weekly during the course of the treatment. All animals were subjected to grip strength, Y maze test, dark light test, tail hanging test, and terminal bone histomorphometry at the end of the treatment. Terminal blood samples were processed for the measurement of immune cell parameters and clinical biochemistry. Several tissues were collected for the measurement of cellular markers of aging hallmarks.

Biochemistry and molecular biology analyses

Serum from mouse of various ages was prepared from blood collected through cardiac puncture in non-heparinized tubes, kept on ice for 10 min, and centrifuged at 15,000 $\times g$ for 10 min at 4 °C. Serum taurine, osteocalcin, and C-terminal telopeptides of Type I collagen degradation products (Ctx) were quantified using ELISA kits—Ctx (Immunodiagnostic Systems PLC), osteocalcin (Immutopics, San Clemente, CA, USA), and taurine (Abbexa Inc., Catalog# abx585011, mouse and monkey)—as described previously (81, 90). Levels of taurine were quantified in serum using ELISA and in tissues using HPLC, as described previously (81). Western blot analysis was performed through standard protocols, as described previously (89).

Liver mitochondrial complex I activity and mtDNA copy number

Mitochondrial complex I activity was analyzed as described previously with minor modifications (123). Briefly, liver tissue was cut over dry ice, weighed, and homogenized 1:180 (weight:volume, mg: μ L) in homogenization buffer (1 mM EDTA and 50 mM triethanolamine) with 2 tungsten beads in a Tissue Lyser (Qiagen cat# 85300), run for 2 cycles of 30 cycles per sec for 1 minute. Mitochondrial complex I (CI, NADH-ubiquinone oxidoreductase) enzymatic activity was quantified spectrophotometrically in 96-well plates on a Spectramax M2 (Spectramax Pro 6, Molecular Devices).

Samples were run in triplicates along with a nonspecific activity control. Complex I activity was determined by measuring the decrease in absorbance of DCIP at 600 nm at 30 °C, in 200 µl of a reaction buffer (potassium phosphate 100mM, pH 7.4) containing 550 mg per ml bovine serum albumin (BSA), 50 mM potassium cyanide (KCN), 20 mM decylubiquinone, and 0.4 mM antimycin A. Ten microliter of homogenate was used to measure CI activity. Antimycin A and KCN were used to inhibit electron flow through complexes III and IV. The negative control condition included rotenone (200 mM) and piericidin A (0.2 mM), which selectively inhibit NADH ubiquinone oxidoreductase. The final CI activity was determined by integrating OD600 change over 250–598 seconds, and by subtracting the rate of NADH oxidation in the presence of rotenone and piericidin A from the total decrease in absorbance. The activity of a single replicate of one sample could not be measured for technical reasons and was therefore not included in the analyses.

Mitochondrial DNA copy number (mtDNAcn) was measured from the same homogenate used for the enzymatic activity measure, lysed at a 1:10 dilution in lysis buffer (114 mM Tris HCl pH 8.5, 6% Tween 20, and 200 µg per ml proteinase K) for 16 hours at 55 °C, 10 minutes at 95 °C, and kept at 4 °C until used for qPCR. Eight microliter of the lysed homogenate was used as template DNA for qPCR. qPCR was performed for triplicate samples in 384 well qPCR plates with 12 µl of master mix in a final reaction volume of 20 µl. Duplex qPCR with Taqman chemistry was used to simultaneously quantify mitochondrial and nuclear amplicons in the same reactions: Cytochrome c oxidase subunit 1 (COX1, mtDNA) and β-2 microglobulin (B2M, nuclear DNA (nDNA)). The Master Mix included 300 nM of primers and 100 nM probe: COX1-Fwd: ACCACCATCATTCTCCTTCTC, COX1-Rev: CTCCTGCATGGCTAGATT, COX1-Probe: HEX/AAGCAGGAG/ZEN/CAGGAACAGGATGAA/3IABkFQ. mB2M-Fwd: GAGAATGGGAAGCCGAACATA, mB2M-Rev: CCGTTCTTCAGCATTGGATT, B2M-Probe: FAM/CGTAACACA/ZEN/GTTCCACCCGCCTC/3IABkFQ. qPCR was performed on a QuantStudio 7 flex instrument (Applied Biosystems Cat# 448570) at 50 °C for 2 min, 95 °C for 20 s, 95 °C for 1 s, 60 °C for 20 s for 40 cycles, with the fluorescence detection threshold for both mitochondrial and nuclear amplicons set to 0.08. Data for triplicates of each sample were averaged for mtDNA and nDNA, and an exclusion cutoff of $C_t > 36$ was applied. For samples with triplicates $C.V.s > 0.02$, the triplicates were checked, outlier values removed where appropriate, and the remaining duplicates were used. The mtDNAcn was derived from the ΔCt calculated by subtracting the average mtDNA Ct from the average nDNA Ct. mtDNAcn was calculated by $2(\Delta Ct) \times 2$ to account for the diploid nuclear genome.

Mitochondrial toxicity assay in worms

Mitochondrial toxin rotenone (a complex I inhibitor) was used to assess the mitochondrial health. A 100 mM stock of rotenone was prepared in the sterile DMSO and stored in small aliquots at -20 °C. From the stock solution, a working solution of rotenone (50 µM) was prepared in S-basal solution (5.85 g per L NaCl, 1 g per L K₂HPO₄, 6 g per L KH₂PO₄, H₂O to 1 L) and dispensed in a 96-well flat-bottom plate (40 µl per well). The rotenone concentration used was based on the previous work (124). All the wells, including control wells were matched to consist 0.05%. Synchronized populations of day-1 adult worms were treated with vehicle or taurine for 7 days and on day 8 worms were picked and transferred to individual wells (10–15 worms per well) containing rotenone. Three hours post-rotenone exposure, worms were scored for motility under the microscope. Values represent mean ± SD.

Clinical studies

Changes in taurine levels with age

Clinical samples used for assessing the changes in taurine levels with age were obtained from the Kuopio Ischaemic Heart Disease Risk Factor Study (KIHD study), a population-based cohort study described previously (81, 125), and were donated by J. Kauhanen and T. Nurmi (University of Eastern Finland, Kuopio, Finland). Clinical samples used for assessing the changes in taurine levels in young subjects were obtained from the Kocaeli University or from the metabolomic studies published earlier by us (126, 127). The ethical research committee of Kocaeli University Hospital approved the protocols (study no. 2013-1, site no. 12), and written consent was obtained from the adults accompanying the subjects, if they were minors.

Clinical risk factors and their association with taurine pathway metabolites

Data from the association matrix were extracted from the open-access web server (<https://omicscience.org/apps/mwasdisease/>) (66). The web server summarizes the results from linear regression models for each of a panel of >50 clinical risk factors, such as prevalence of type 2 diabetes, with over 1000 metabolites that were quantified in 11,966 subjects from the EPIC-Norfolk study (128) in an untargeted metabolomics approach (Metabolon HD4 platform). Metabolite levels were corrected for age, sex, fasting time, and time of blood sampling. Detailed methods for this characterization are described elsewhere (66). Summary statistics, including standardized regression coefficients (β -estimates) and nominal p -values on a relevant subset of 26 clinical traits and three taurine-related metabolites were extracted from this web server. Regression coefficients and nominal p -values were plotted in a heatmap using R version 4.1.0.

Measurement of taurine and other metabolites in a human exercise cohort

Taurine, hypotaurine, and N-acetyltaurine levels were measured in the serum of four different subject groups (three groups of competitive athletes and one sedentary control group) of healthy young males ($n = 35$), before and after a maximum graded exercise (cardiopulmonary exercise testing, CPET) on a bicycle ergometer. The study was approved by the medical ethics committee of the Technical University of Munich (356/17S). Participants were fully informed of the nature and possible risks of the study before they gave their written informed consent and were fully informed that their data will be made publicly available to the scientific community after anonymization. All athletes in this study were competing at a national level in their respective discipline and engaging in sports-specific training for at least 8 h a week. Sedentary subjects ($n = 7$) were engaging in a maximum of 45 min of exercise a week. Athlete groups were recruited to depict maximum phenotypic and metabolic contrast between the highly oxidative metabolism of endurance athletes ($n = 11$) and their high proportion of slow twitch type 1 muscle fibers versus the high capacity to build muscle mass (anabolism) and the high amount of muscle mass itself in natural bodybuilders ($n = 9$) versus the highly glycolytic metabolism and high proportion of fast twitch type 2 muscle fibers in sprinters ($n = 8$). Baseline blood samples were drawn at 07:00 am in the morning after a 10 h fasting overnight. Detailed methods for a subcohort of this study are described elsewhere (129). Briefly, 10 min after baseline blood sampling, the subjects exercised on a stationary bicycle ergometer at a linearly increasing load of 30 W per min until voluntary exhaustion. Post-exercise blood samples were taken exactly 5 min after voluntary exhaustion. Blood was drawn using a butterfly cannula into a 9 ml serum gel collecting tubes (S-Monovette, Sarstedt, Germany). Blood was allowed to clot for 30 min at room temperature (~22–24 °C) and then centrifuged for 10 min at 2,460 × g at 15 °C to prepare serum. Thereafter, serum was collected in 1.0 ml cryotubes (Sarstedt, Germany) and stored at –80 °C until analysis. Blood sera from baseline and from post-exercise groups were analyzed using LC-MS employing an untargeted metabolomics approach (Metabolon Inc., Durham, NC, USA). The resulting raw ion count data were median batch corrected per metabolite and log₂ transformed. Technical measurement

variability, as determined by coefficient of variation after batch correction in reference samples, was below 25%. Differences between baseline and post-exercise metabolite levels were analyzed per subject group using a paired sample *t*-test. Batch correction and log₂-transformation were done using R version 4.1.0 and paired sample *t*-test and the graph preparation were done using GraphPad Prism version 9.1.2.

Monkeys, treatment, and experimental design

Studies in monkeys were approved by the Institutional Animal Ethics Committee of the National Institute of Immunology and Large Animals Committee (NII; file number: 25/31/2017-CPCSEA). All the methods were performed in accordance with the guidelines and regulations of the Committee for the Purpose of Control and Supervision of Experiments on Animals, India and adhered to the ARRIVE guidelines (130) under the supervision of a professional veterinarian at the Primate Research Facility of NII, New Delhi. Rhesus monkeys (*Macaca mulatta*) were individually housed in standard primate cages at the large animal facility, National Institute of Immunology, New Delhi, India. Animals were maintained under standard environmental conditions (24 ± 2.1 °C, 55%–60% relative humidity, 12:12h dark:light photoperiod) and housed individually in stainless-steel non-human primate cages. Young (5.0 ± 1.8 y) and aged (15.0 ± 1.5 y) *M. mulatta* females were used in the present study. Young monkeys were used for the measurement of serum taurine levels depicted in Fig. 1B. All animals had access to Certified Global Primate Diet (PMI Nutrition International, Inc.), containing 0.93% calcium, 0.75% phosphorus, and 8.0 IU of vitamin D₃ per g, twice daily, as well as to daily food supplements including fresh fruit. We note that the monkey diet contains taurine, albeit at very low levels (~0.01%). The animal room environment was controlled, with 24 ± 3 °C temperature, $50\% \pm 20\%$ relative humidity, 12:12 h dark:light photoperiod, and 12 air changes per hour. Only animals considered in good health, and with normal serum/urine chemistry panels were used in the study. Rhesus monkeys show irregularity in the age at which cessation of menstrual cyclicity (menopause) occurs, which often compounds analyses done in old monkeys due to varying levels of ovarian steroids present. To circumvent this issue, and to generate a non-human primate model of aging in females as close to human physiology as possible, all animals were subjected to bilateral ovariectomy through laparotomy under anesthesia (ketamine:xylazine) few weeks before the start of vehicle or taurine administration. Monkeys were assigned randomly to a vehicle or taurine-treatment group. Vehicle (PBS, $n = 7$) or taurine in a banana paste embedded in a bread roll was given immediately before the morning meal. All animals were first trained for 1 month through daily supplementation of banana paste embedded in bread roll to ensure complete consumption of the dose to be given prior to initiation of experiments. After the start of the treatment regimen, the experimentalist stayed in the room till the time monkeys completely consumed the given banana and ensured that it was not discarded to the floor. The groups were balanced by baseline body weight and confirmed to have similar mean baseline lumbar BMD and BMC by DEXA (figs. S7 E to F). The study was terminated on day 181 when animals were anesthetized with ketamine/xylazine and transported to Mahajan Imaging Facility for DEXA scans of the total spine (L1–L4), head, and leg, and changes in % fat mass using a Lunar DPX-L densitometer. A pediatric software from GE healthcare was used to analyze the baseline and post-treatment bone density in vehicle- and taurine-treated monkeys. The entire scan was performed by a signal operator for better precision. A schematic diagram of the chronology of different tests in monkeys is presented in fig. S7D.

Serum levels of taurine and biochemical markers of bone turnover in monkeys

Blood samples were collected at 3- and 6-month after administration of vehicle or taurine. Animals were random-fed prior to blood sampling on all occasions except for the assessment of fasting

blood glucose levels for which animals were bled before giving the first meal of the day. The bone-formation marker, osteocalcin (Ocn), was measured by radioimmunoassay (Ocn: DSL-6900, Diagnostic System Laboratories, USA). The bone-resorption marker, serum C-telopeptide (CTX), was quantified using a Serum Crosslaps ELISA.

5 **Bone densitometry by DEXA in monkeys**

Prior to scanning, monkeys were first sedated with an injection of a cocktail of glycopyrrolate, ketamine hydrochloric acid (HCl), and xylazine and transported to the imaging facility. Animals were administered another dose of anesthesia, if required. Areal BMC and BMD of the lumbar spine (L1–L4), head, and legs were measured using DEXA (Lunar DPX-L densitometer) at the baseline (predose 1) and on day 181. The precision [coefficient of variation (CV, %)] of DEXA scanning with repositioning ranged from 0.8% at the lumbar spine to 4.5% at the leg.

10 **Statistical analysis**

All values are depicted as mean \pm SEM. Data were estimated to be statistically significant at $p \leq 0.05$. $p \leq 0.0001****$, $p \leq 0.001***$, $p \leq 0.01**$, and $p \leq 0.05*$ are versus WT or control. Statistical parameters including the exact value of n , post hoc test for each figure are listed below.

15 **Main manuscript Figures:**

20 **Figure 1:** The OASIS software (<http://sbi.postech.ac.kr/oasis>) was used and p -values were calculated using a log rank (the Mantel–Cox method) test for statistical analyses of survivability in mice and worms. Wilcoxon rank-sum test was used by for calculating p -values to determine the statistical significance in yeast RLS assays.

25 **Figure 2:** Statistical analysis was performed using Graph Pad Prism 7 and data were considered statistically significant at $p \leq 0.05$ using the Student's t -test, one-way, or two-way ANOVA.

30 **Figure 3:** The OASIS software (<http://sbi.postech.ac.kr/oasis>) was used and p -values were calculated using a log rank (the Mantel–Cox method) test for statistical analyses of survivability in mouse and fish experiments (panels D, G, I). For other panels, statistical analysis was performed using Graph Pad Prism 7 and data were considered statistically significant at $p \leq 0.05$ using Student's t -test, one-way, or two-way ANOVA.

35 **Figure 4:** Statistical analysis in human association studies (A): Summary statistics, including standardized regression coefficients (β -estimates) and nominal p -values on a relevant subset of 26 clinical traits and three taurine-related metabolites were extracted from this web server. Regression coefficients and nominal p -values were plotted in a heatmap using R version 4.1.0. Statistical analysis for the exercise cohort (B-D): Differences between baseline and post-exercise metabolite levels were analyzed per subject group using a paired sample t -test. Batch correction and log₂-transformation were done using R version 4.1.0 and paired sample t -test; the graphs were prepared using GraphPad Prism. For other panels (E-O), statistical analysis was performed using Graph Pad Prism 7 and data were considered statistically significant at $p \leq 0.05$ using the Student's t -test one-way ANOVA or two-way ANOVA.

40 **Supplemental figures S1-7:** Each figure legend contains the statistical methods.

Supplemental figures:

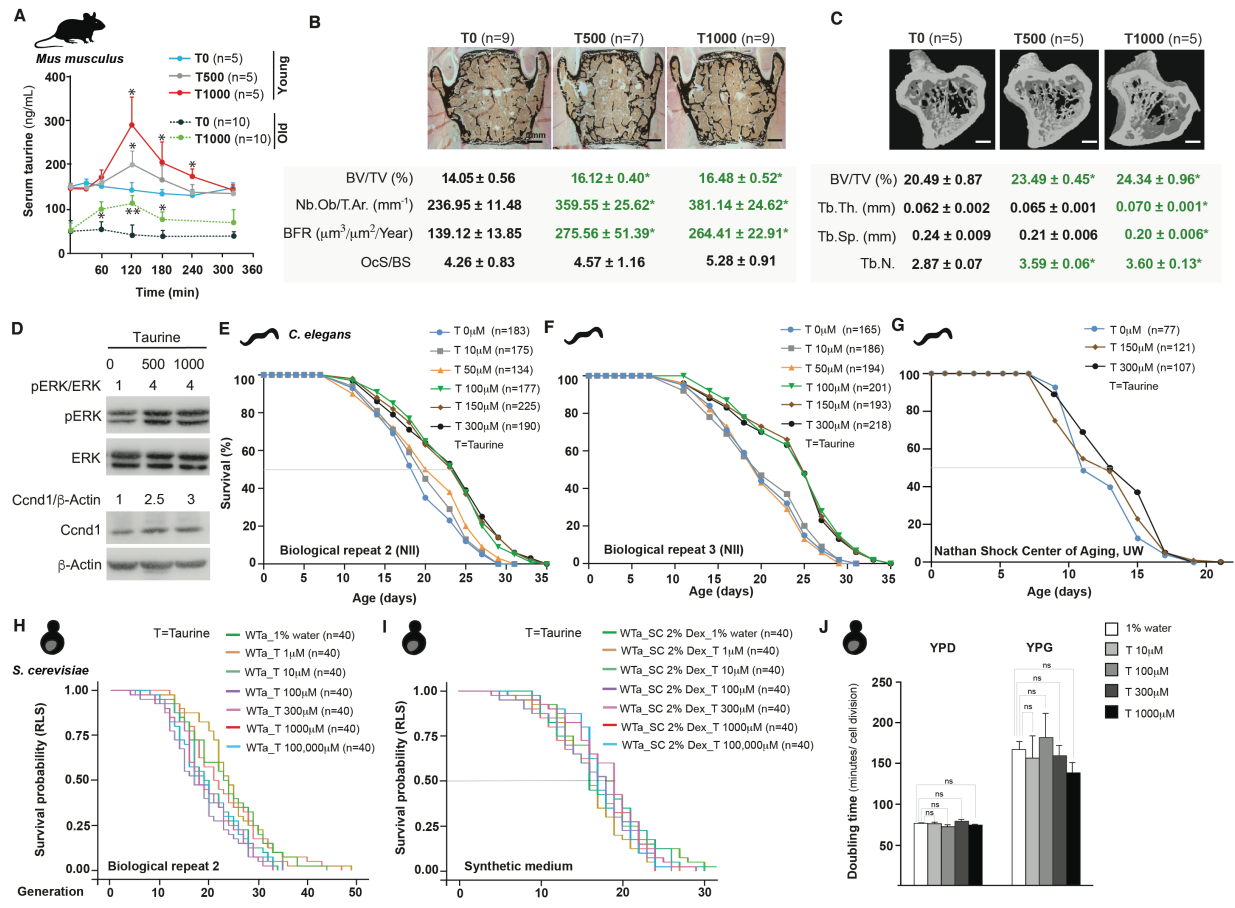


Figure S1

fig. S1. Taurine is a driver of aging in evolutionarily divergent species. (A) Serum taurine levels at different time points following oral gavage of 0, 500, or 1000 mg per kg body weight per day taurine (T0, 500, or T1000) in 1- and 14-month-old wild type mice. (B-D) Histological and histomorphometric analysis of vertebra (B), μCT analysis of long bone femur (C), and ERK phosphorylation and Ccnd1 levels in long bone (D), following 6 weeks of daily vehicle (T0) or taurine administration at T500 or T1000 in wild-type mice. (E-G) Biological repeats of lifespan assay of WT nematodes fed normal dead *Escherichia coli* OP50 diet (ND) or ND supplemented with different doses of taurine (0, 10, 50, 100, 150, and 300 μM). The lifespan assays were performed at National Institute of Immunology (NII) or at Nathan Shock Center of Aging, University of Washington. (H-I) Replicative lifespan (RLS) assay (biological replication of assay in Fig. 1G) in yeast cultured on YPD plates (H) or on synthetic medium (I) with different concentrations of taurine (0, 1, 10, 100, 300, 1000, and 100,000 μM). (J) Yeast doubling time in YPD and YPG media with different concentrations of taurine (0, 1, 10, 100, 300, and 1000 μM). Values are mean ± SEM. n is represented for each experimental group analyzed. The OASIS software (<http://sbi.postech.ac.kr/oasis>) was used and p-values were calculated using a log rank (the Mantel–Cox method) test for statistical analyses of survivability in mice and worms. Wilcoxon rank-sum test was used by for calculating p values to determine statistical significance in yeast RLS assays. For the other panels, statistical analysis was performed using Graph Pad Prism 7 and data were estimated to be statistically significant at $p \leq 0.05$ using the Student's t-test, one-way, or two-way ANOVA. * $p < 0.05$; ** $p < 0.01$ compared with T0.

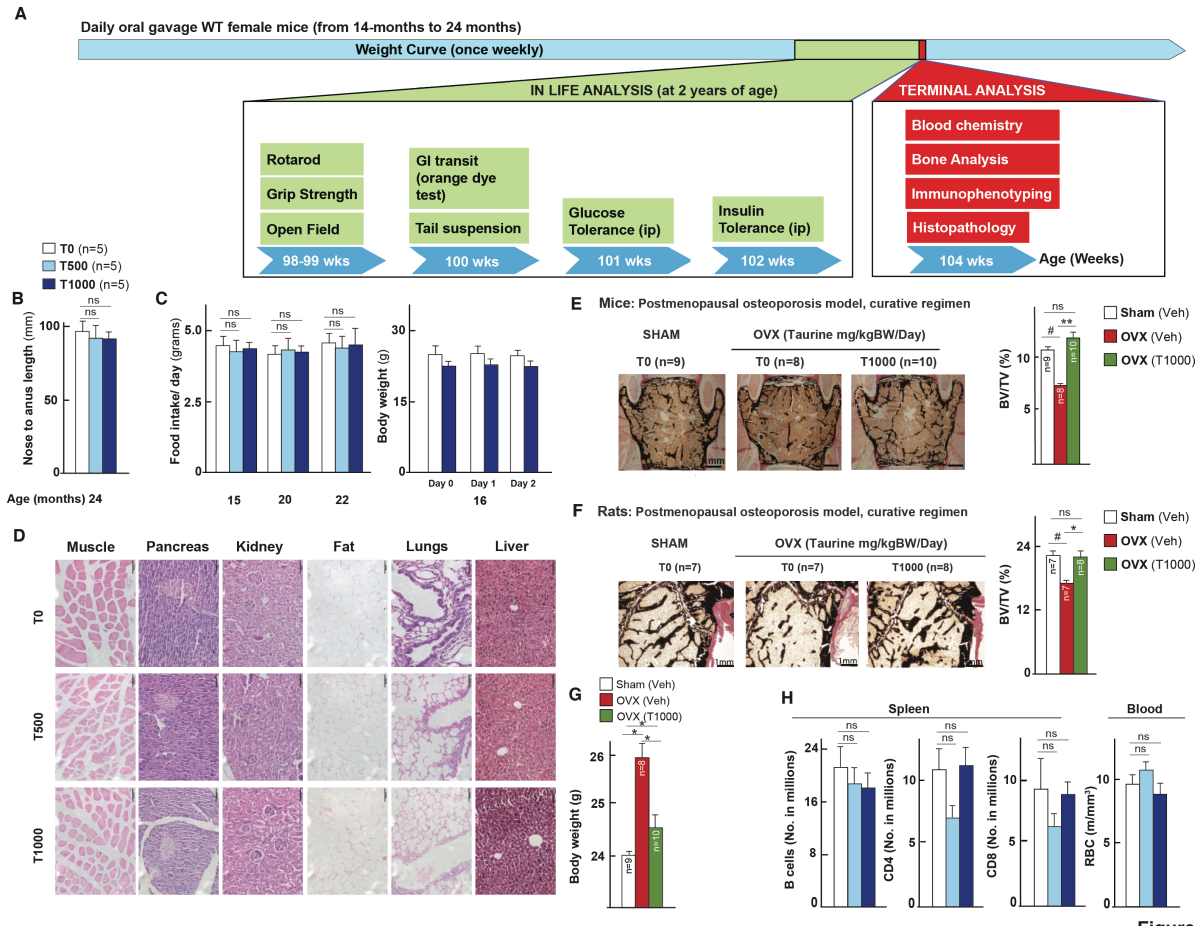


Figure S2

fig. S2. Taurine increases healthspan in middle-aged female mice. (A) Schematic representation of the experimental regimen, and the order of in-life and terminal assays to investigate the effect of taurine supplementation from the middle-age (14 months) for 12 months on muscle function (rotarod and grip strength tests), memory (open field test), gastrointestinal transit (orange dye test), anxiety (tail suspension test), pancreas function (glucose and insulin tolerance test), immune system function (immunophenotyping), bone structure, and changes in organ histopathology in female wild type mice. (B-D) Changes in nose-to-anus length (B), food intake and changes in body weight during food intake measurement at indicated ages (C), and histopathology (D) in 24-month-old wild-type (WT) C57Bl/6J mice orally fed vehicle (T0) or taurine (T500, or T1000) once daily from 14-months of age. (E) Von Kossa-stained vertebral sections and BV/TV% in sham or ovariectomized (OVX) mice, left untreated for 6 weeks to develop osteopenia and then treated in a curative mode with vehicle or T1000 for 6 weeks. (F) Von Kossa-stained femur sections and BV/TV% in 12 weeks-old sham or ovariectomized rats, left untreated for 6 weeks to develop osteopenia and then treated in a curative mode daily with vehicle or T1000 for 12 weeks. (G) Terminal body weight in sham or ovariectomized (OVX) mice, left untreated for 6 weeks to develop osteopenia and then treated in a curative mode with vehicle or T1000 for 6 weeks. (H) Changes in immune cell parameters in the spleen or blood of 24-month-old WT C57Bl/6J female mice orally fed taurine (T0, 500, or 1000), once daily, from 14-months of age. n is represented for each experimental group analyzed. Values are mean \pm SEM. Statistical analysis was performed using Graph Pad Prism 7 and data were estimated to be statistically

significant at $p \leq 0.05$ using the Student's t -test, one-way, or two-way ANOVA. ns, not significant; * $p < 0.05$; ** $p < 0.01$ compared with T0.

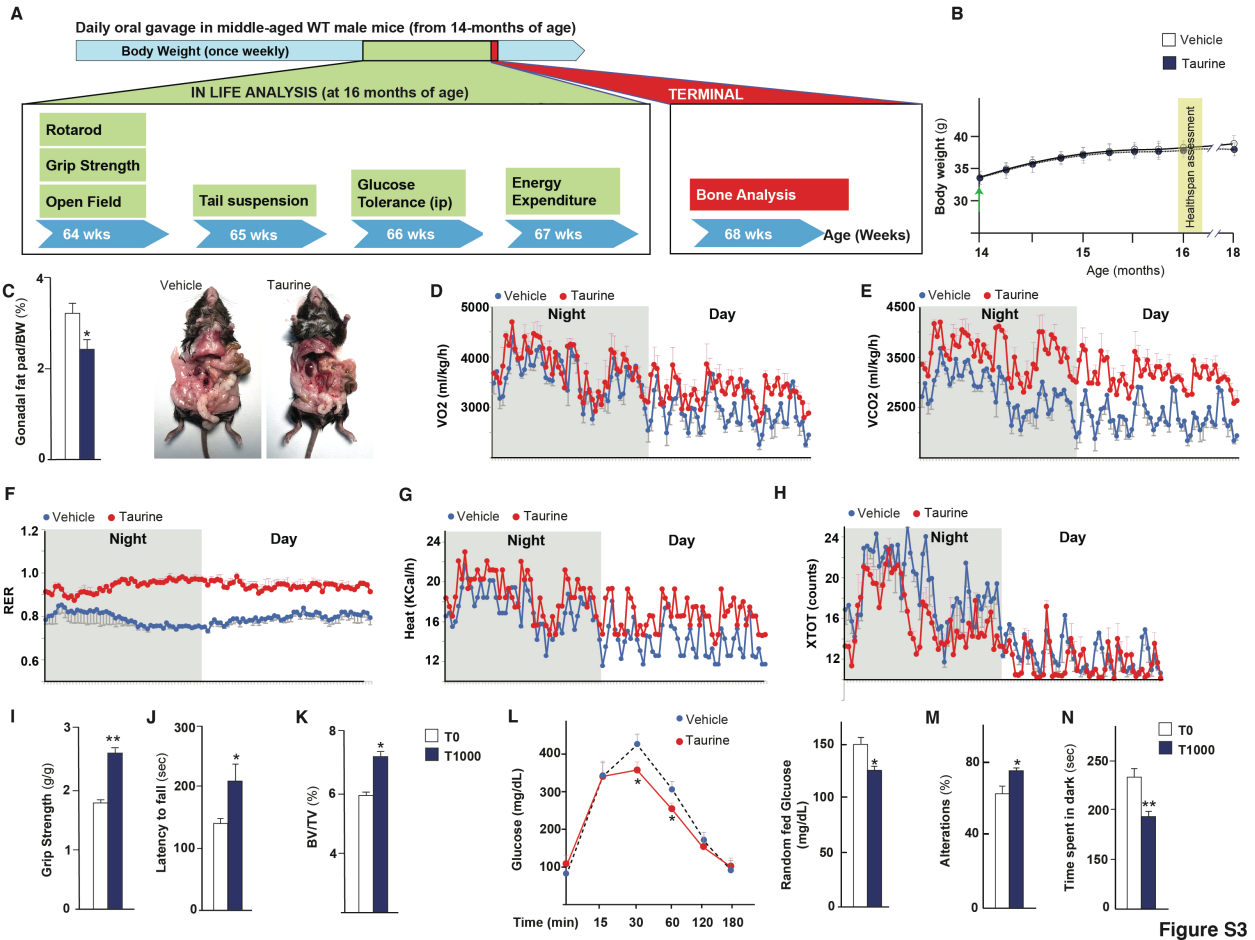


Figure S3

fig. S3. Taurine increases healthy lifespan in middle-aged WT male mice. A) Schematic representation of the experimental regimen, and the order of in-life and terminal assays to investigate the effect of taurine supplementation from the middle-age (14 months) on body weight acquisition, muscle function (rotarod and grip strength tests), memory (open field test), anxiety (tail suspension test), pancreas function (glucose tolerance test), and bone structure. (B-M) Changes in body weight (B), Fat % and representative photomicrographs (C), Volume of oxygen consumed (VO₂, D), volume of CO₂ produced (VCO₂, E), respiratory exchange ratio (RER, F), heat production (G), XTOT (H), muscle strength (grip strength, I), neuromuscular function (rotarod test, J), bone mass [bone volume over total volume % in vertebra (BV/TV%), K], pancreas function (L, glucose tolerance test), memory (M, Y maze test), and anxiety (N, dark-light tests) in 16- to 18-month-old wild-type C57Bl/6J male mice orally fed taurine (T0 or 1000) once daily from middle-age (14 months). *n* is represented for each experimental group analyzed. Values are mean \pm SEM. Statistical analysis was performed using Graph Pad Prism 7 and data were estimated to be statistically significant at $p \leq 0.05$ using the Student's *t*-test, one-way, or two-way ANOVA. ns, not significant; * $p < 0.05$; ** $p < 0.01$ compared with T0.

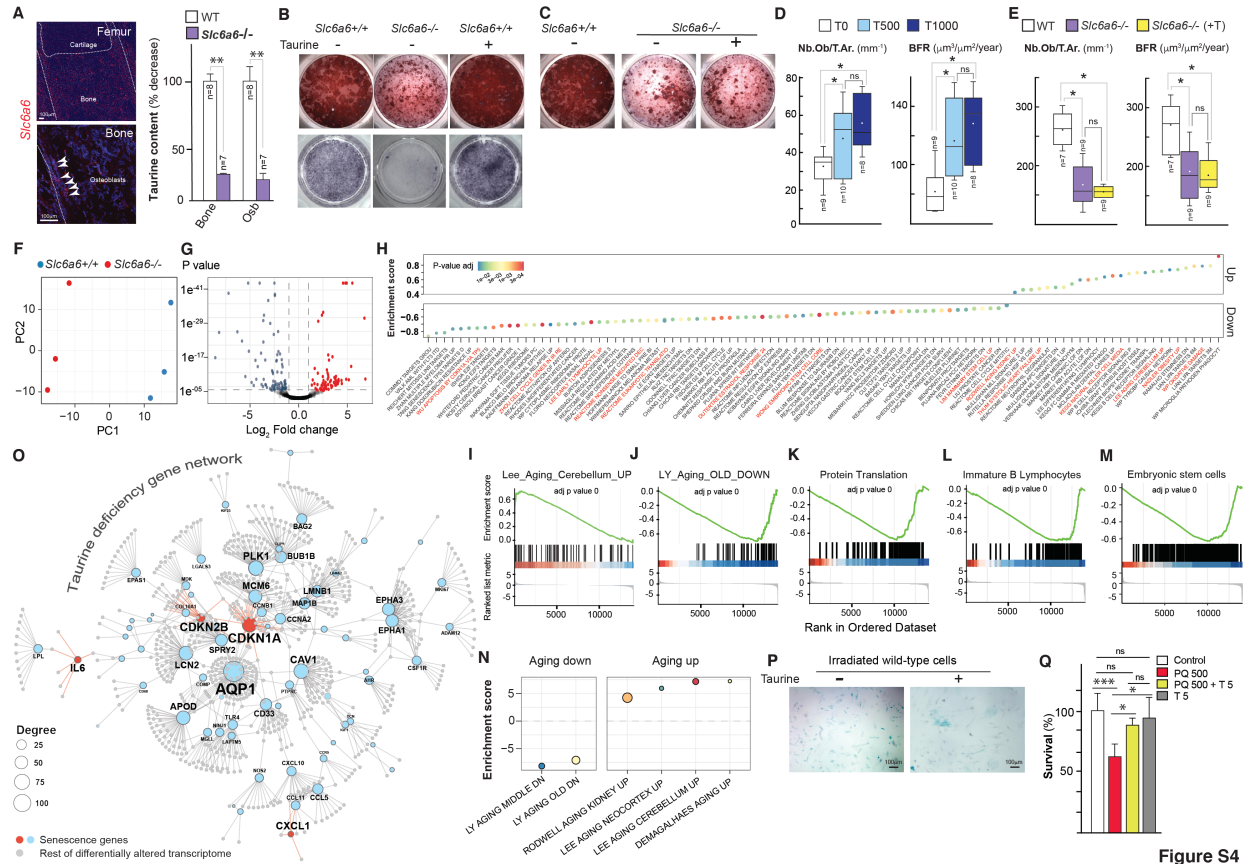


Figure S4

fig. S4. Taurine regulates classical hallmarks of aging in mice.

(A) In situ hybridization analysis of *Slc6a6* expression in the wild-type (WT) bone and relative taurine content in the bone and primary osteoblasts (Osb) of WT and *Slc6a6*^{-/-} mice. (B) Mineralization (top panels) and differentiation (bottom panels) assay in wild-type (WT, *Slc6a6*^{+/+}) and taurine-deficient (*Slc6a6*^{-/-}) osteoblasts cultured in vehicle- or taurine-supplemented medium. (C) Mineralization assay in WT (+/+) and *Slc6a6*^{-/-} osteoblasts cultured with vehicle or taurine-supplemented medium. (D-E) Analysis of the number of osteoblasts and bone formation rate in the vertebral sections from middle-aged WT female mice that received vehicle or taurine at T500 or T1000 for 12 months (D), and in vertebral sections from WT and *Slc6a6*^{-/-} female mice treated with vehicle or taurine (E). (F-L) WT and *Slc6a6*^{-/-} osteoblasts were prepared from mouse calvaria and total RNA was subjected to RNA-seq analysis ($n = 3$ per group). Principal component analysis (F), volcano plot (G), ensemble of gene set enrichment analysis (EGSEA) (H), selected GSEA plots (I-M) and aging term enrichment in GSEA (N) in taurine-deficient osteoblast transcriptome. (O) Senescence gene network forms critical nodes in taurine-deficient transcriptome. In red are senescence associated secretory phenotype (SASP) markers. (P) Senescence associated β-galactosidase (SA-β-Gal) staining (blue-stained cells) of irradiated primary osteoblasts with or without taurine supplementation, from two representative experiments. (Q) Survival analysis of primary N2 neurons cultured with vehicle or taurine (at 5 mM, T5) following paraquat (PQ)-induced senescence. n is represented for each experimental group analyzed. Values are mean ± SEM for all panels except for panel Q (mean ± SD). Statistical analysis was performed using Graph Pad Prism 7 and data were estimated to be statistically significant at $p \leq 0.05$ using the Student's *t*-test, one-way, or two-way ANOVA. ns, not significant; * $p < 0.05$; ** $p < 0.01$; *** $p < 0.001$; **** $p < 0.0001$ compared with controls.

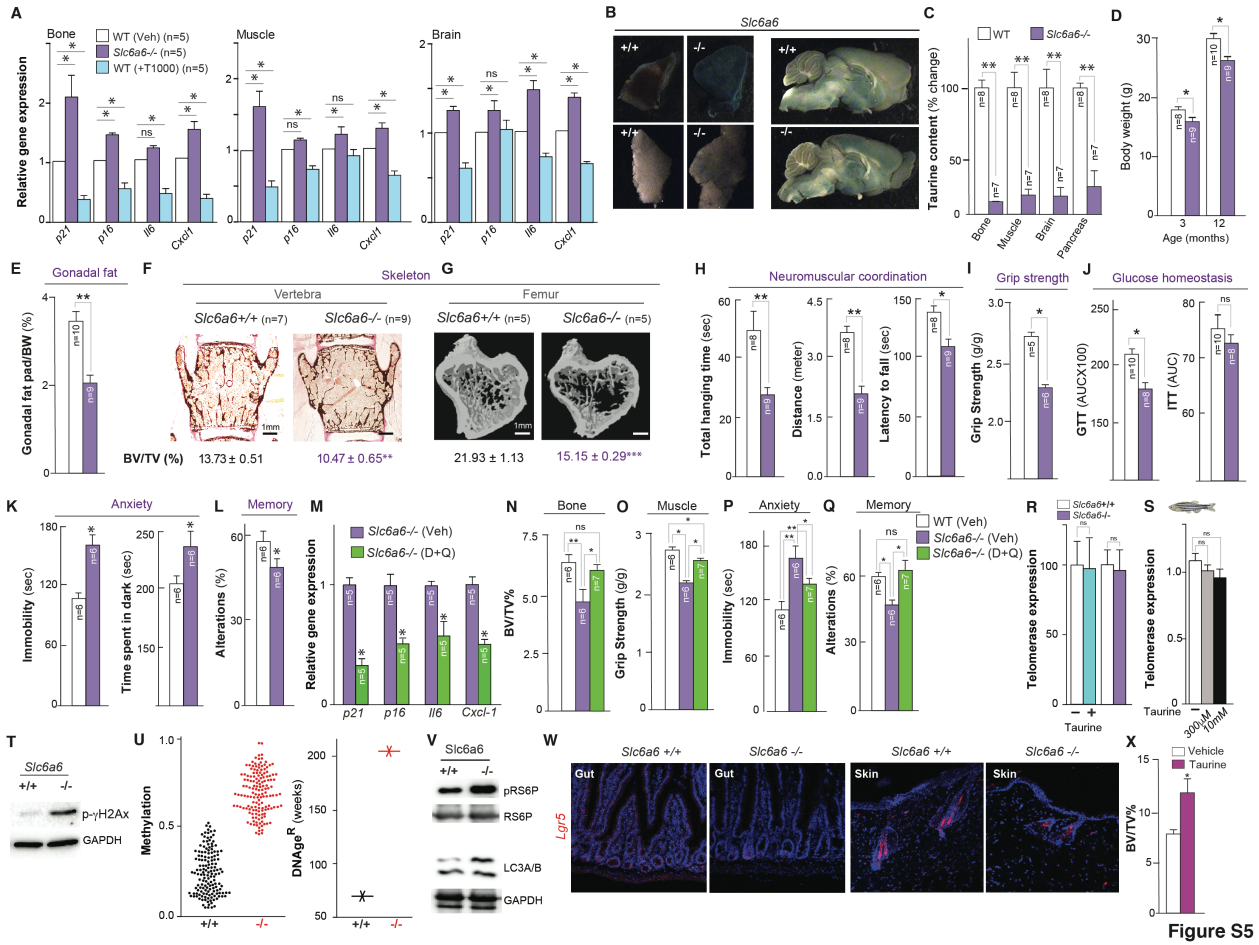


Figure S5

fig. S5. Congenitally taurine-deficient mice display several hallmarks of aging during adult hood. (A) Analysis of SASP markers in different tissues collected from wild-type (WT) and *Slc6a6*^{-/-} mice, and in middle-aged WT mice that received vehicle or T1000 for 12 months. (B) Senescence associated β-galactosidase (SA-β-Gal) staining (blue-stained cells) in tissues collected from WT and *Slc6a6*^{-/-} mice. (C) % change in tissue taurine content in tissues collected from WT and *Slc6a6*^{-/-} mice. (D-L) Changes in body weight (D), Fat % (E), bone structure in spine and long bones (F-G), neuromuscular and muscle strength (H-I, rotarod, wire hang, and grip-strength tests), pancreas function (J), glucose and insulin tolerance tests, area under the curve is shown for each group), anxiety (K, tail suspension and dark-light tests), and memory (L, Y maze test) in *Slc6a6*^{-/-} mice and littermate controls. (M-Q) Changes in SASP marker genes expression (M), bone mass (N, bone volume over total volume %), muscle function (O, grip-strength test), anxiety (P, tail suspension test), and memory (Q, Y maze test) in 12-month-old *Slc6a6*^{-/-} and littermate controls that received either vehicle or a combination of senolytics (dasatinib [D] + quercetin [Q]) biweekly, for 4 months. (R) Telomerase gene expression in the liver of vehicle- and taurine-treated mice and in *Slc6a6*^{-/-} mice. (S) Telomerase gene expression in WT fish embryos treated with taurine. (T-W) Phospho-γ-H2Ax levels in skeletal muscle (T), DNA methylation level of significantly different loci and DNA methylation age (U), Changes in phospho-ribosomal S6 protein (pRS6P) and LC3A/B in muscle (V), and in situ hybridization analysis of expression changes in *Lgr5*, a gene expressed in stem or progenitor cells of the gut and skin (W) of WT or *Slc6a6*^{-/-} mice. (X) Bone mass (BV/TV%) in 4-week-old offspring born from mothers that received either vehicle or T1000 during gestation from embryonic day 0.5 to birth. *n* = 6–10 mice

in each group. Values are mean \pm SEM. Statistical analysis was performed using Graph Pad Prism 7 and data were estimated to be statistically significant at $p \leq 0.05$ using the Student's *t*-test, one-way, or two-way ANOVA. ns, not significant; * $p < 0.05$; ** $p < 0.01$ compared with controls.

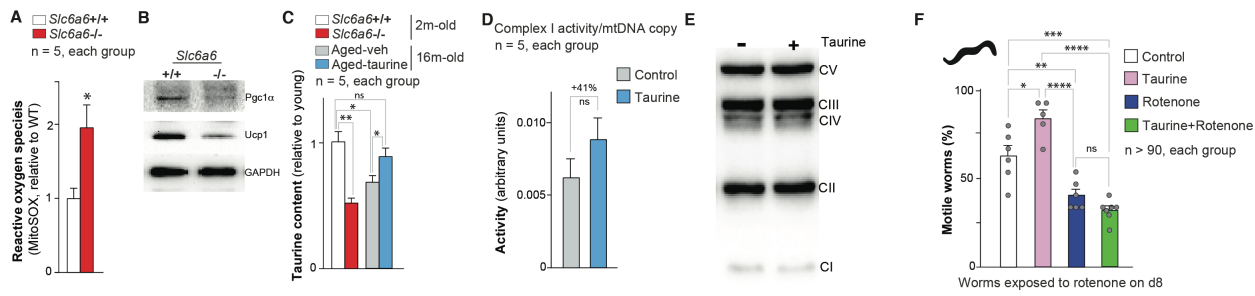


Figure S6

5

10

15

fig. S6. Taurine regulates mitochondrial health in mice. (A-B) levels of mitochondrial ROS (superoxide anion radicals, MitoSOX assay) in skeletal muscle mitochondria (A), and Pgc1 α and Ucp1 levels in the brown fat (B) of wild-type (WT, *Slc6a6^{+/+}*) and taurine-deficient (*Slc6a6^{-/-}*) mice. (C) Changes in liver taurine content in young 2-month-old WT and *Slc6a6^{-/-}* mice, and aged 16-month-old mice that received vehicle or taurine for 8 weeks. (D-E) Levels of mitochondrial complex I activity per mitochondrial DNA copy (D), and levels of OXPHOS mitochondrial complex proteins (E) in middle-aged WT mice that received either vehicle or T1000. (F) Rotenone-induced complex I inhibition assay on worms grown on vehicle or taurine supplemented plates. n > 90 worms in each group. Western blots are representative of three independent biological replicates. Values are mean \pm SEM for all panels except for panels D and F (mean \pm SD). Statistical analysis was performed using Graph Pad Prism 7 and data were estimated to be statistically significant at $p \leq 0.05$ using the Student's *t*-test, one-way, or two-way ANOVA. ns, not significant; * $p < 0.05$; ** $p < 0.01$; *** $p < 0.001$; **** $p < 0.0001$ compared with controls.

20

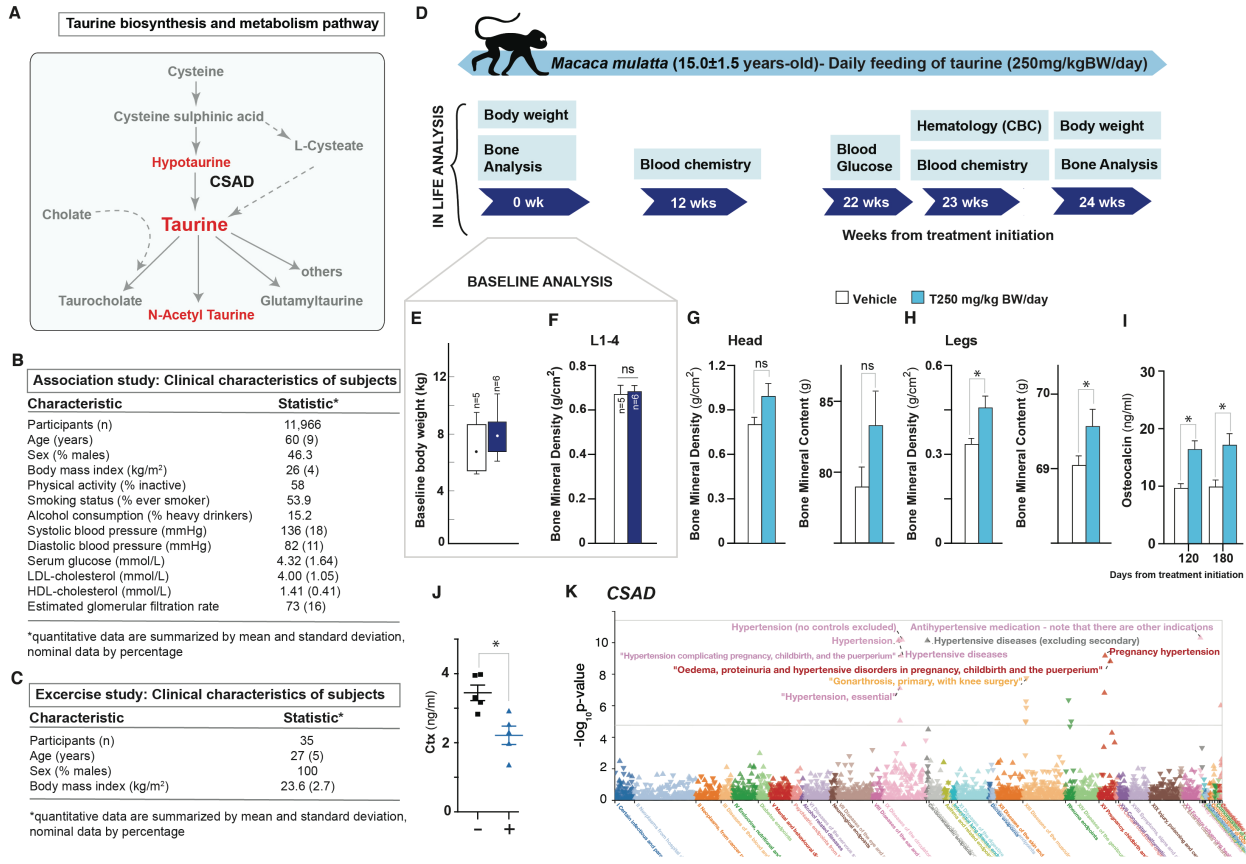


Figure S7

fig. S7. Taurine pathway regulates healthspan in primates. (A) Pathways for taurine biosynthesis and metabolism in humans. Taurine-related metabolites measured in blood from 11,966 subjects are shown in red for clinical risk association in the EPIC-Norfolk study. (B) Clinical characteristics of subjects in the EPIC-Norfolk study. (C) Clinical characteristics of subjects in the exercise study. (D) Schematic representation of the chronology of in-life tests to investigate the effect of once daily taurine supplementation for 6 months in 15-year-old monkeys (equivalent to ~45–50-year-old humans) compared with vehicle-treated controls on body weight, bone formation and resorption markers in the blood, pancreas function (fasting blood glucose levels), immune system function (immunophenotyping), and bone structure (DEXA analysis). (E–F) Baseline difference in body weight (E) and bone mineral density at lumbar 1–4 vertebra (F) in monkeys of the two groups prior to the start of treatment. (G–J) bone mineral density and content in head (G) legs (H), and serum levels of bone formation marker, osteocalcin (I), and bone resorption marker, Ctx (J) in 15-year-old monkeys orally fed once daily with vehicle (T0) or taurine (T250) for 6 months. (K) Phenome-wide plot showing association at the CSAD locus with hypertension and gonarthrosis in the FinnGen database (release 5). n is represented for each experimental group analyzed. Values are mean \pm SEM. Statistical analysis was performed using Graph Pad Prism 7 and data were estimated to be statistically significant at $p \leq 0.05$ using the Student's *t*-test, one-way, or two-way ANOVA. ns, not significant; * $p < 0.05$ compared with controls.

Table S1.

Enrichment of aging gene signatures in the transcriptome of taurine-deficient cells. The six gene signatures that showed significant alterations in the GSEA pathways are presented. All six signatures show expected direction of change (up or down-regulation) for a pro-aging effect of taurine deficiency.

Pathway	Description	Reference	Genes
LEE_AGING_C EREBELLUM_UP	Upregulated in the cerebellum of aged adult mice (30-month) vs. young adult (5-month)	https://pubmed.ncbi.nlm.nih.gov/10888876/	DNAJB2,GNB2,APOE,B2M,RHOG,SIPA1L2,CTS S,CST7,AGT,GCK,CTSZ,IARS1,IFI27,IMPA1,HN RNPH3,TRAPPC5,CTSS,PTBP2,EIF2B5,,SEZ6,W DFY3,RPSA,TRIM5,GFAP,THBS2,SLC11A1,BCL 2A1,LGALS3BP,MPEG1,EPS15,MYH8,TYMS,C 4B,C1QB,OR2C1,APC,SNTA1,CTSH,IRGM,UBE 2H,EFS,TBC1D1,MNAT1,PTPRO,ACADVL,IFIT1 B,GBP4,NOS3,TBX6,SLC7A3,IRF7,HSPA8,FOS, HLA-DQB1,TGFBR3,AGT,PIGF,GNG11,EPRS1,CAPN 2,,CCL21,FCRL2,ITGB5,CDK4,NOTCH1,IGHM, HOXA4,SPP1,LMNB1,LGALS3,NR4A1,F2,CTSD ,NFYA,BDNF,HMOX1,HOXD12,C1QA,AXL,C1Q C,CD68,CD24,AMH,PGLYRP1,SELPLG,HEXB
RODWELL_AGING_KIDNEY_UP	Genes down-regulated in fibroblasts from old individuals, compared to those from young donors	https://pubmed.ncbi.nlm.nih.gov/10741968/	CCL5,RPL35,RPL28,FAU,RPL18,RPL27,KXD1,RPL 12,RPS25,RPS10,LASP1,PFN1,P4HB,GRN,RPL13 A,RPL10,RHOA,CALU,SPARCL1,HLA-E,HLA- E,RPLP2,TAGLN2,CCND2,CCND2,SERPING1,SSR 4,RPN1,SYNGR2,MGAT1,GPNMB,ITPR3,ARHGD IB,STAT6,VIM,TGFBI,IRAK1,ANXA2,IFITM1,TNC, TIMP1,CCND3,LAPTM5,LAPTM5,CD14,LUM,PS ME2,AEBP1,VARS1,MYOF,LPCAT1,COL3A1,SRG N,UBXN1,ARPC1B,LTF,ARHGAP1,LY6E,CELF2,M VP,PLOD3,ARL4C,NNMT,NNMT,TAP1,COL1A1, PAM,CFB,COL1A2,COL1A2,TNFAIP2,LYN,RPS19 ,PSMB10,AXL,FBN1,SLC1A3,ITGB2,ABCC1,TRA F D1,ADGRE5,C1QB,HCLS1,RGS1,C7,LTBR,CHST1 5,CSF1R,APRT,RPS6KA1,CD53,RBP1,TPBG,COL 15A1,RTN1,LOXL1,EMP3,STS,VSNL1,IL32,VCA M1,MMP11,PIK3CD,IRF9,WFDC2,NT5E,VASH1, CLDN3,IRF8,PLAAT4,MYRF,TYROBP,LIG3,STAB1 ,CDO1,IFNAR1,RUNX3,TMEM243,GMFG,FCER1 G,MMP7,PSMB9,PROM1,RGS10,TMC6,RGS19, MRC1,ALOX5,CXCL1,C15orf39,GABRE,RAD54L, NUAK1,CCL5,HLA-DRB1,STOML1,EVI2A,FAS,HLA-

		F,BTN3A3,TYMP,ARHGAP25,IL10RA,TNFRSF11B,TNFRSF11B,NCF1,GABRP,ASNS,CRIP1,CCR1,QPCT,ADAM8,LCP2,AMBP,GZMA,TAGLN,GGT5,LY75,BCL2A1,CD38,COMP,ARVCF,CD1D,SLC18A2,TREX1,GABBR1,CX3CR1,RAB33A,PIK3CG,CTS6,GZMK,CLEC10A,PTPN6,RBMS3,MIOS,FLT3L,TPSAB1,CDH11,HTATIP2,ISLR,LTB,SCN5A,THEMIS2,ADGRE2,NUP62,PRB1,FDXR,SNCA,HTR7,VOPP1,TBXAS1,PCDHA9,HLA-DRB1,C4A,POU4F3,ACTN1,ACTN1,PDIA4,CLIC1,TKT,HLA-B,C1S,HLA-B,TAPBP,TMED3,HLA-DRA,PSMB8,CORO1A,TSPAN1,TUBA1A,IGLC2,HLA-B,AATF,MAN2B1,WDR46,DEGS1,HLA-DRB1,IKBKB,MALL,IGHM,HTATIP2,NR2F1,ARHGEF6,LDLRAD4,MOXD1,CD69,HLA-DQB1,ADRA2A,SELPLG,VEGFC,HGF,ANXA2,FN1,HLA-G,BIRC3,MFGE8,LST1,FEZ2,TCF3,THEMIS2,TRBC1,FSCN1,HLA-DRA,TPM1,TPM1,PRUNE1,DOK1,ANXA2P3,GRN,MCAM,CASP1,CASP1,CASP1,IGHG1,HLA-G,HLA-G,HLA-G,SNCA,LST1,CHRNA3,IGHV3-23,HLA-DQB1,HLA-DQB1,FN1,FYB1,TRBC2,HLA-B,HLA-DPA1,HLA-DPA1,PXDN,C1R,ADGRG1,SERPINE2,FNBP1,SEL1L3,ZCCHC24,FN1,COL5A1,MAP4,PTPRC,PTPRC,JCHAIN,RFTN1,FKBP15,HLA-DQA1,PPP1R14B,RPL13A,C1orf216,TBC1D2B,IGHM,ARHGAP45,EML3,HLA-DQB1,CHI3L2,DOCK2,SVEP1,TFPI,TRIM22,CA5BP1,RPS19,ANXA2,RAB3GAP1,RNASE6,RAC2,LAMP1,MYO1F,TCF3,KCND3,CD47,NKG7,HLA-A,LYZ,SPON1,SPON1,IFITM1,NCF1,LST1,DKK3,CN3,INSL3,C4A,HLA-B,LST1,IGLC2,SLC46A3,IGKV2D-28,MSR1,CDH6,NRXN3,COL3A1,IGLC2,IGKV1D-39,HLA-DRB1,HLA-A,IGLC2,LST1,FAS,SHANK2,IGLL3P,GRN,TBCB,RPL18AP16,FN1,HLA-B,IGHV3-21,RPL10P17,CCL2,RGS1,RRP12,IGHA1,CXCR4,KIAA0930,IGHV3-47,HLA-DRB6,IGKV1OR2-108,HLA-J,HLA-E,HLA-DMA,TYMP,MILR1,TMSB10,A2M,RAB31,TME43,CXCL14,RPS27L,C20orf27,CYBC1,PLEKHO1,C1QA,CRELD2,PGLS,FHOD1,PARP12,DPP3,DR
--	--	---

			AM1,SPON2,REEP4,TESC,RIGI,TMPRSS4,CORO7,MICALL2,PGGHG,SLAMF8,TNFRSF25,ARHGA P10,RUBCNL,MARCHF1,SLC15A3,TOR4A,VTCN1,CLEC4A,IL17B,SLC12A9,IKZF1,ITM2C,TXNDC5,BHLHE41,CALHM2,IGKC,IGKC,CLEC7A,VCAN,MYDGF,EHBP1L1,RPS2,CHPF2,RBCK1,PTPRE,RARRES1,HLA-F,COL8A2,NLGN4X,CORO1C,NUB1,CLDN1,ACER3,TPM3,SHISA5,SLC40A1,CCM2,GASK1B,NFKBIZ,MS4A6A,RASSF5,MS4A7,ABRACL,BLOC1S4,CXCL16,C15orf48,DOK3,HCST,SNHG12,FXYD5,MS4A6A,MS4A7,GPR61,ANTXR1,PARP14,RAB34,SULF2,CMTM3,ASAP1,IGKC,POLR1D,KRTCAP2,CARHSP1,ZFAS1,STING1,PREX1,PPP1R18,SETD7,STING1,GNG2,CCDC88A,MRAS,RPL35A,COL27A1,C1QC,VSIR,DTX3L,MTHFD1L,ANTXR2,GLIPR2,CTHRC1,AKNA,GNB4,ZMAT3,JAZF1,TRIM47,RNF213,RNF213,DPCD,CMTM7,USP31,PPM1M,PIGR,ARHGAP30,NLRC5,ZCCHC7,SAMD9L,DGKQ,OSMR,RAB8B,SVBP,SLFN5,ITGA1,SLFN11,LYSMD2,FIBIN,ATP8B2,MPEG1,MPEG1,DOCK11,RFLNB,PPP1R14A,LEPROT,IFNAR2,INHBA,FYB1,IKBIP,TSPAN18,NFIX,GFRA1,GPX8,SOCS3,RNF166,SPTLC3,NAPSB,JAML,ZMAT3,ZEB2,ALPK2,GGTA1,RAB4B,SAMD9,COL14A1,SLC6A6,LACC1,ITGB2-AS1,IL17RA,PGM2L1,IL17RA,CALHM6,GBP5,NUS1,,C4orf48,ERICH3,RNF213,SAMD9L,TM4SF18,CYRIA,HIKESHI,RHEX,SLFN5,CXorf38,MS4A6A,PRICKLE1,ST8SIA4,LIX1,APBB1IP,IL4I1,KLF8,TIMP2,IRAK2,PALD1,RNF213,GIMAP2,RUNX2,DPPI3,SYTL2,PARVG,ADCY10P1,LDLRAD3,SAMHD1,PRAG1,RNF125,MARCHF1,DLGAP1,SAMHD1,MIR34AHG,SAMHD1,PTPN22,CANX,ODF3B,RP27L,FZD3,LINC02086,SCARNA17,C7,RNF213,CARD8-AS1,VWCE,UBE2Q2P16,HAVCR1,LMF2,SYMPK,STK10,RUBCNL,LDLRAP1,RIN3,UBE2D4,ZNF783
LY_AGING_OLD_D_DN	Genes down-regulated in fibroblasts from old individual	https://pubmed.ncbi.nlm.nih.gov/10741968/	PSMD11,PSMD12,TYMS,PSMA2,PSMA3,PSMC2,POSTN,MCM2,CDH11,KIF14,PTGS2,RANBP1,CKAP5,TGFBR2,UGCG,PSMC6,PARP1,PCNA,PTGS2,SAFB,CCNB1,FBL,SERPINB2,H2AZ1,NASP,CDC25B,PLK1,FBN2,PTGS2,CDC20,CENPA,CENPF,CSE1L,CDK4,KIF11,ATR,NAE1,HAS2,PKMYT1,KIF2C,PAFAH1B1,UBE2C,HSD17B10,FOXM1,BAR

	s, compared to those from young donors		D1,DDX39A,MYBL2,HMGN2,H2AX,CCNA2,CKS 1B,HMGB2,KIF23,PPP1CC,CTSC,CXCL8,NUP88, CCNF
DEMAGALHAE S_AGING_UP	Genes consistently overexpressed with age, based on meta-analysis of microarray data	https://pubmed.ncbi.nlm.nih.gov/19189975/	NDRG1,GPNMB,VAT1,NPC2,TXNIP,PTGES3,HC ST,TMED10,CLU,CTSS,MPEG1,EFEMP1,FCGR2A ,FCGR2B,RASA3,CLIC4,GBP2,GFAP,GNS,GSTA1, H1-2,HBA1,ANXA3,ANXA5,HLA-G,APOD,JCHAIN,DCLK1,LGALS3,LYZ,MGST1,MS N,MT1F,PCSK6,B2M,PSMD11,RNF213,S100A4, S100A6,SGK1,SPP1,SERPING1,C1QA,C1QB,C1QC,C3,C4A,VWF,LAPTM5,DERL1,ADIPOR2,IL33,LTAF,EFCAB14
LEE_AGING_N EOCORTEX_UP	Upregulated in the neocortex of aged adult mice (30-month) vs. young adult (5-month)	https://pubmed.ncbi.nlm.nih.gov/10888876/	ATP1B3,PPP1R2,COX8BP,,NAPA,HSD17B12,B2M,DNAJB13,WWOX,DNAJA4,RHOG,PSAT1,DNAH8,CTSS,ZNF14,TUBB,EEF2,CSNK1G2,CMPK1,CTSZ,SEC23B,IFI27,SET,DLG1,ICAM2,RUFY1,RB14,DHX15,CSNK1D,FXYD6,RRAGA,VPS72,JUNB,LCAT,GFAP,CD9,SAT1,LGALS3BP,MPEG1,GA DD45A,APOD,LAMB1,C4B,,VIM,MAG,PTGS1,C RYAB,AVP,OXT,CTNNB1,VEGFA,P4HA1,CYB561 ,STOM,STXBP3,AKT2,NUB1,PPP2R5C,NDRG1,V AMP1,FOS,UBC,ALDOC,S100A10,CCL21,RAB4A ,SPP1,NR4A1,CTSD,C1QA,M6PR,C1QC,DDIT3,C D68,ITIH3,PHB1,SEMA4B,KCNA1
LY_AGING_MI DDLE_DN	Genes down-regulated in fibroblasts from middle-age individuals, compared to those from the young donors	https://pubmed.ncbi.nlm.nih.gov/10741968/	PTGS2,CCNB1,PLK1,CDC20,CENPA,CENPF,KIF11,KIF2C,UBE2C,FOXM1,MYBL2,HMGN2,H2AX,CCNA2,KIF23,CCNF

References and Notes

1. Department of Economic and Social Affairs of the United Nations, Population Division, “World population ageing 2019: Highlights” (ST/ESA/SER.A/430, United Nations, 2019);
<https://www.un.org/en/development/desa/population/publications/pdf/ageing/WorldPopulationAgeing2019-Highlights.pdf>.
2. G. V. Mkrtchyan, K. Abdelmohsen, P. Andreux, I. Bagdonaitė, N. Barzilai, S. Brunak, F. Cabreiro, R. de Cabo, J. Campisi, A. M. Cuervo, M. Demaria, C. Y. Ewald, E. F. Fang, R. Faragher, L. Ferrucci, A. Freund, C. G. Silva-García, A. Georgievskaya, V. N. Gladyshev, D. J. Glass, V. Gorbunova, A. de Grey, W.-W. He, J. Hoeijmakers, E. Hoffmann, S. Horvath, R. H. Houtkooper, M. K. Jensen, M. B. Jensen, A. Kane, M. Kassem, P. de Keizer, B. Kennedy, G. Karsenty, D. W. Lamming, K.-F. Lee, N. MacAulay, P. Mamoshina, J. Mellon, M. Molenaars, A. Moskalev, A. Mund, L. Niedernhofer, B. Osborne, H. H. Pak, A. Parkhitko, N. Raimundo, T. A. Rando, L. J. Rasmussen, C. Reis, C. G. Riedel, A. Franco-Romero, B. Schumacher, D. A. Sinclair, Y. Suh, P. R. Taub, D. Toiber, J. T. Treebak, D. R. Valenzano, E. Verdin, J. Vijg, S. Young, L. Zhang, D. Bakula, A. Zhavoronkov, M. Scheibye-Knudsen, ARDD 2020: From aging mechanisms to interventions. *Aging* **12**, 24484–24503 (2020).
[doi:10.18632/aging.202454](https://doi.org/10.18632/aging.202454) [Medline](#)
3. D. Gems, L. Partridge, Genetics of longevity in model organisms: Debates and paradigm shifts. *Annu. Rev. Physiol.* **75**, 621–644 (2013). [doi:10.1146/annurev-physiol-030212-183712](https://doi.org/10.1146/annurev-physiol-030212-183712) [Medline](#)
4. J. Campisi, P. Kapahi, G. J. Lithgow, S. Melov, J. C. Newman, E. Verdin, From discoveries in ageing research to therapeutics for healthy ageing. *Nature* **571**, 183–192 (2019).
[doi:10.1038/s41586-019-1365-2](https://doi.org/10.1038/s41586-019-1365-2) [Medline](#)
5. K. Meyer, B. A. Yankner, Slowing down aging. *Cell Metab.* **26**, 592–593 (2017).
[doi:10.1016/j.cmet.2017.09.012](https://doi.org/10.1016/j.cmet.2017.09.012) [Medline](#)
6. H. Pan, T. Finkel, Key proteins and pathways that regulate lifespan. *J. Biol. Chem.* **292**, 6452–6460 (2017). [doi:10.1074/jbc.R116.771915](https://doi.org/10.1074/jbc.R116.771915) [Medline](#)
7. M. C. Haigis, B. A. Yankner, The aging stress response. *Mol. Cell* **40**, 333–344 (2010).
[doi:10.1016/j.molcel.2010.10.002](https://doi.org/10.1016/j.molcel.2010.10.002) [Medline](#)
8. T. A. Rando, H. Y. Chang, Aging, rejuvenation, and epigenetic reprogramming: Resetting the aging clock. *Cell* **148**, 46–57 (2012). [doi:10.1016/j.cell.2012.01.003](https://doi.org/10.1016/j.cell.2012.01.003) [Medline](#)
9. E. H. Blackburn, C. W. Greider, J. W. Szostak, Telomeres and telomerase: The path from maize, Tetrahymena and yeast to human cancer and aging. *Nat. Med.* **12**, 1133–1138 (2006). [doi:10.1038/nm1006-1133](https://doi.org/10.1038/nm1006-1133) [Medline](#)
10. D. W. Lamming, L. Ye, D. M. Sabatini, J. A. Baur, Rapalogs and mTOR inhibitors as anti-aging therapeutics. *J. Clin. Invest.* **123**, 980–989 (2013). [doi:10.1172/JCI64099](https://doi.org/10.1172/JCI64099) [Medline](#)
11. W. A. Cabral, U. L. Tavarez, I. Beeram, D. Yeritsyan, Y. D. Boku, M. A. Eckhaus, A. Nazarian, M. R. Erdos, F. S. Collins, Genetic reduction of mTOR extends lifespan in a mouse model of Hutchinson-Gilford progeria syndrome. *Aging Cell* **20**, e13457 (2021).
[doi:10.1111/ace.13457](https://doi.org/10.1111/ace.13457) [Medline](#)

12. L. J. Niedernhofer, P. D. Robbins, Senotherapeutics for healthy ageing. *Nat. Rev. Drug Discov.* **17**, 377 (2018). [doi:10.1038/nrd.2018.44](https://doi.org/10.1038/nrd.2018.44) [Medline](#)
13. C. López-Otín, M. A. Blasco, L. Partridge, M. Serrano, G. Kroemer, The hallmarks of aging. *Cell* **153**, 1194–1217 (2013). [doi:10.1016/j.cell.2013.05.039](https://doi.org/10.1016/j.cell.2013.05.039) [Medline](#)
14. T. B. Kirkwood, Understanding the odd science of aging. *Cell* **120**, 437–447 (2005). [doi:10.1016/j.cell.2005.01.027](https://doi.org/10.1016/j.cell.2005.01.027) [Medline](#)
15. S. I. Imai, L. Guarente, It takes two to tango: NAD⁺ and sirtuins in aging/longevity control. *NPJ Aging Mech. Dis.* **2**, 16017 (2016). [doi:10.1038/npjamd.2016.17](https://doi.org/10.1038/npjamd.2016.17) [Medline](#)
16. Y. Zhang, Y. Xie, E. D. Berglund, K. C. Coate, T. T. He, T. Katafuchi, G. Xiao, M. J. Potthoff, W. Wei, Y. Wan, R. T. Yu, R. M. Evans, S. A. Kliewer, D. J. Mangelsdorf, The starvation hormone, fibroblast growth factor-21, extends lifespan in mice. *eLife* **1**, e00065 (2012). [doi:10.7554/eLife.00065](https://doi.org/10.7554/eLife.00065) [Medline](#)
17. A. Asadi Shahmirzadi, D. Edgar, C.-Y. Liao, Y.-M. Hsu, M. Lucanic, A. Asadi Shahmirzadi, C. D. Wiley, G. Gan, D. E. Kim, H. G. Kasler, C. Kuehnemann, B. Kaplowitz, D. Bhaumik, R. R. Riley, B. K. Kennedy, G. J. Lithgow, Alpha-ketoglutarate, an endogenous metabolite, extends lifespan and compresses morbidity in aging mice. *Cell Metab.* **32**, 447–456.e6 (2020). [doi:10.1016/j.cmet.2020.08.004](https://doi.org/10.1016/j.cmet.2020.08.004) [Medline](#)
18. H. Ripps, W. Shen, Review: taurine: a “very essential” amino acid. *Mol. Vis.* **18**, 2673–2686 (2012). [Medline](#)
19. L. L. Spriet, J. Whitfield, Taurine and skeletal muscle function. *Curr. Opin. Clin. Nutr. Metab. Care* **18**, 96–101 (2015). [doi:10.1097/MCO.0000000000000135](https://doi.org/10.1097/MCO.0000000000000135) [Medline](#)
20. I. H. Lambert, D. M. Kristensen, J. B. Holm, O. H. Mortensen, Physiological role of taurine—From organism to organelle. *Acta Physiol.* **213**, 191–212 (2015). [doi:10.1111/apha.12365](https://doi.org/10.1111/apha.12365) [Medline](#)
21. A. Hébert, M.-P. Forquin-Gomez, A. Roux, J. Aubert, C. Junot, J.-F. Heilier, S. Landaud, P. Bonnarme, J.-M. Beckerich, New insights into sulfur metabolism in yeasts as revealed by studies of *Yarrowia lipolytica*. *Appl. Environ. Microbiol.* **79**, 1200–1211 (2013). [doi:10.1128/AEM.03259-12](https://doi.org/10.1128/AEM.03259-12) [Medline](#)
22. F. G. Tiedemann, Einige neue Bestandtheile der Galle des Ochsen. *Ann. Physik. Chem.* **9**, 326–337 (1827).
23. U. Warskulat, B. Heller-Stilb, E. Oermann, K. Zilles, H. Haas, F. Lang, D. Häussinger, Phenotype of the taurine transporter knockout mouse. *Methods Enzymol.* **428**, 439–458 (2007). [doi:10.1016/S0076-6879\(07\)28025-5](https://doi.org/10.1016/S0076-6879(07)28025-5) [Medline](#)
24. J. G. Jacobsen, L. H. Smith, Biochemistry and physiology of taurine and taurine derivatives. *Physiol. Rev.* **48**, 424–511 (1968). [doi:10.1152/physrev.1968.48.2.424](https://doi.org/10.1152/physrev.1968.48.2.424) [Medline](#)
25. K. C. Hayes, R. E. Carey, S. Y. Schmidt, Retinal degeneration associated with taurine deficiency in the cat. *Science* **188**, 949–951 (1975). [doi:10.1126/science.1138364](https://doi.org/10.1126/science.1138364) [Medline](#)
26. M. N. Preising, B. Görg, C. Friedburg, N. Qvartskhava, B. S. Budde, M. Bonus, M. R. Toliat, C. Pfleger, J. Altmüller, D. Herebian, M. Beyer, H. J. Zöllner, H.-J. Wittsack, J. Schaper, D. Klee, U. Zechner, P. Nürnberg, J. Schipper, A. Schnitzler, H. Gohlke, B. Lorenz, D.

- Häussinger, H. J. Bolz, Biallelic mutation of human *SLC6A6* encoding the taurine transporter TAUT is linked to early retinal degeneration. *FASEB J.* **33**, 11507–11527 (2019). [doi:10.1096/fj.201900914RR](https://doi.org/10.1096/fj.201900914RR) Medline
27. B. Eppler, R. Dawson Jr., Dietary taurine manipulations in aged male Fischer 344 rat tissue: Taurine concentration, taurine biosynthesis, and oxidative markers. *Biochem. Pharmacol.* **62**, 29–39 (2001). [doi:10.1016/S0006-2952\(01\)00647-5](https://doi.org/10.1016/S0006-2952(01)00647-5) Medline
28. H. J. Stuerenburg, B. Stangneth, B. G. Schoser, Age related profiles of free amino acids in human skeletal muscle. *Neuroendocrinol. Lett.* **27**, 133–136 (2006). [Medline](#)
29. L. M. Suárez, M. D. Muñoz, R. Martín Del Río, J. M. Solís, Taurine content in different brain structures during ageing: Effect on hippocampal synaptic plasticity. *Amino Acids* **48**, 1199–1208 (2016). [doi:10.1007/s00726-015-2155-2](https://doi.org/10.1007/s00726-015-2155-2) Medline
30. T. Yoshimura, Y. Inokuchi, C. Mutou, T. Sakurai, T. Nagahama, S. Murakami, Age-related decline in the taurine content of the skin in rodents. *Amino Acids* **53**, 429–434 (2021). [doi:10.1007/s00726-021-02956-2](https://doi.org/10.1007/s00726-021-02956-2) Medline
31. E. M. Carneiro, M. Q. Latorraca, E. Araujo, M. Beltrá, M. J. Oliveras, M. Navarro, G. Berná, F. J. Bedoya, L. A. Velloso, B. Soria, F. Martín, Taurine supplementation modulates glucose homeostasis and islet function. *J. Nutr. Biochem.* **20**, 503–511 (2009). [doi:10.1016/j.jnutbio.2008.05.008](https://doi.org/10.1016/j.jnutbio.2008.05.008) Medline
32. K. Fukuda, Y. Nishi, T. Usui, Free amino acid concentrations in plasma, erythrocytes, granulocytes, and lymphocytes in umbilical cord blood, children, and adults. *J. Pediatr. Gastroenterol. Nutr.* **3**, 432–439 (1984). [doi:10.1097/00005176-198406000-00022](https://doi.org/10.1097/00005176-198406000-00022) Medline
33. M. Jeevanandam, D. H. Young, L. Ramias, W. R. Schiller, Effect of major trauma on plasma free amino acid concentrations in geriatric patients. *Am. J. Clin. Nutr.* **51**, 1040–1045 (1990). [doi:10.1093/ajcn/51.6.1040](https://doi.org/10.1093/ajcn/51.6.1040) Medline
34. B. N. Ames, Prolonging healthy aging: Longevity vitamins and proteins. *Proc. Natl. Acad. Sci. U.S.A.* **115**, 10836–10844 (2018). [doi:10.1073/pnas.1809045115](https://doi.org/10.1073/pnas.1809045115) Medline
35. T. Ito, N. Yoshikawa, T. Inui, N. Miyazaki, S. W. Schaffer, J. Azuma, Tissue depletion of taurine accelerates skeletal muscle senescence and leads to early death in mice. *PLOS ONE* **9**, e107409 (2014). [doi:10.1371/journal.pone.0107409](https://doi.org/10.1371/journal.pone.0107409) Medline
36. L. S. Yilmaz, X. Li, S. Nanda, B. Fox, F. Schroeder, A. J. M. Walhout, Modeling tissue-relevant *Caenorhabditis elegans* metabolism at network, pathway, reaction, and metabolite levels. *Mol. Syst. Biol.* **16**, e9649 (2020). [doi:10.15252/msb.20209649](https://doi.org/10.15252/msb.20209649) Medline
37. Q. L. Wan, X. Shi, J. Liu, A.-J. Ding, Y.-Z. Pu, Z. Li, G.-S. Wu, H.-R. Luo, Metabolomic signature associated with reproduction-regulated aging in *Caenorhabditis elegans*. *Aging* **9**, 447–474 (2017). [doi:10.18632/aging.101170](https://doi.org/10.18632/aging.101170) Medline
38. M. A. McCormick, J. R. Delaney, M. Tsuchiya, S. Tsuchiyama, A. Shemorry, S. Sim, A. C.-Z. Chou, U. Ahmed, D. Carr, C. J. Murakami, J. Schleit, G. L. Sutphin, B. M. Wasko, C. F. Bennett, A. M. Wang, B. Olsen, R. P. Beyer, T. K. Bammler, D. Prunkard, S. C. Johnson, J. K. Pennypacker, E. An, A. Anies, A. S. Castanza, E. Choi, N. Dang, S. Enerio, M. Fletcher, L. Fox, S. Goswami, S. A. Higgins, M. A. Holmberg, D. Hu, J. Hui,

- M. Jelic, K.-S. Jeong, E. Johnston, E. O. Kerr, J. Kim, D. Kim, K. Kirkland, S. Klum, S. Kotireddy, E. Liao, M. Lim, M. S. Lin, W. C. Lo, D. Lockshon, H. A. Miller, R. M. Moller, B. Muller, J. Oakes, D. N. Pak, Z. J. Peng, K. M. Pham, T. G. Pollard, P. Pradeep, D. Pruitt, D. Rai, B. Robison, A. A. Rodriguez, B. Ros, M. Sage, M. K. Singh, E. D. Smith, K. Snead, A. Solanky, B. L. Spector, K. K. Steffen, B. N. Tchao, M. K. Ting, H. Vander Wende, D. Wang, K. L. Welton, E. A. Westman, R. B. Brem, X. G. Liu, Y. Suh, Z. Zhou, M. Kaeberlein, B. K. Kennedy, A comprehensive analysis of replicative lifespan in 4,698 single-gene deletion strains uncovers conserved mechanisms of aging. *Cell Metab.* **22**, 895–906 (2015). [doi:10.1016/j.cmet.2015.09.008](https://doi.org/10.1016/j.cmet.2015.09.008) [Medline](#)
39. S. T. Coleman, T. K. Fang, S. A. Rovinsky, F. J. Turano, W. S. Moye-Rowley, Expression of a glutamate decarboxylase homologue is required for normal oxidative stress tolerance in *Saccharomyces cerevisiae*. *J. Biol. Chem.* **276**, 244–250 (2001). [doi:10.1074/jbc.M007103200](https://doi.org/10.1074/jbc.M007103200) [Medline](#)
40. S. J. Olshansky, From lifespan to healthspan. *JAMA* **320**, 1323–1324 (2018). [doi:10.1001/jama.2018.12621](https://doi.org/10.1001/jama.2018.12621) [Medline](#)
41. H. Shoji, K. Takao, S. Hattori, T. Miyakawa, Age-related changes in behavior in C57BL/6J mice from young adulthood to middle age. *Mol. Brain* **9**, 11 (2016). [doi:10.1186/s13041-016-0191-9](https://doi.org/10.1186/s13041-016-0191-9) [Medline](#)
42. L. Steru, R. Chermat, B. Thierry, P. Simon, The tail suspension test: A new method for screening antidepressants in mice. *Psychopharmacology* **85**, 367–370 (1985). [doi:10.1007/BF00428203](https://doi.org/10.1007/BF00428203) [Medline](#)
43. M. Bourin, M. Hascoët, The mouse light/dark box test. *Eur. J. Pharmacol.* **463**, 55–65 (2003). [doi:10.1016/S0014-2999\(03\)01274-3](https://doi.org/10.1016/S0014-2999(03)01274-3) [Medline](#)
44. E. Pavlopoulos, S. Jones, S. Kosmidis, M. Close, C. Kim, O. Kovalerchik, S. A. Small, E. R. Kandel, Molecular mechanism for age-related memory loss: The histone-binding protein RbAp48. *Sci. Transl. Med.* **5**, 200ra115 (2013). [doi:10.1126/scitranslmed.3006373](https://doi.org/10.1126/scitranslmed.3006373) [Medline](#)
45. N. Dey, V. E. Wagner, L. V. Blanton, J. Cheng, L. Fontana, R. Haque, T. Ahmed, J. I. Gordon, Regulators of gut motility revealed by a gnotobiotic model of diet-microbiome interactions related to travel. *Cell* **163**, 95–107 (2015). [doi:10.1016/j.cell.2015.08.059](https://doi.org/10.1016/j.cell.2015.08.059) [Medline](#)
46. J. M. Yano, K. Yu, G. P. Donaldson, G. G. Shastri, P. Ann, L. Ma, C. R. Nagler, R. F. Ismagilov, S. K. Mazmanian, E. Y. Hsiao, Indigenous bacteria from the gut microbiota regulate host serotonin biosynthesis. *Cell* **161**, 264–276 (2015). [doi:10.1016/j.cell.2015.02.047](https://doi.org/10.1016/j.cell.2015.02.047) [Medline](#)
47. R. H. Cho, H. B. Sieburg, C. E. Muller-Sieburg, A new mechanism for the aging of hematopoietic stem cells: Aging changes the clonal composition of the stem cell compartment but not individual stem cells. *Blood* **111**, 5553–5561 (2008). [doi:10.1182/blood-2007-11-123547](https://doi.org/10.1182/blood-2007-11-123547) [Medline](#)
48. S. Mangiola, R. Molania, R. Dong, M. A. Doyle, A. T. Papenfuss, tidybulk: An R tidy framework for modular transcriptomic data analysis. *Genome Biol.* **22**, 42 (2021). [doi:10.1186/s13059-020-02233-7](https://doi.org/10.1186/s13059-020-02233-7) [Medline](#)

49. S. J. Chinta, G. Woods, M. Demaria, A. Rane, Y. Zou, A. McQuade, S. Rajagopalan, C. Limbad, D. T. Madden, J. Campisi, J. K. Andersen, Cellular senescence is induced by the environmental neurotoxin paraquat and contributes to neuropathology linked to Parkinson's disease. *Cell Rep.* **22**, 930–940 (2018). [doi:10.1016/j.celrep.2017.12.092](https://doi.org/10.1016/j.celrep.2017.12.092) [Medline](#)
50. J. S. Yi, Y. Huang, A. T. Kwaczala, I. Y. Kuo, B. E. Ehrlich, S. G. Campbell, F. J. Giordano, A. M. Bennett, Low-dose dasatinib rescues cardiac function in Noonan syndrome. *JCI Insight* **1**, e90220 (2016). [doi:10.1172/jci.insight.90220](https://doi.org/10.1172/jci.insight.90220) [Medline](#)
51. M. J. McEachern, A. Krauskopf, E. H. Blackburn, Telomeres and their control. *Annu. Rev. Genet.* **34**, 331–358 (2000). [doi:10.1146/annurev.genet.34.1.331](https://doi.org/10.1146/annurev.genet.34.1.331) [Medline](#)
52. C. M. Henriques, M. C. Carneiro, I. M. Tenente, A. Jacinto, M. G. Ferreira, Telomerase is required for zebrafish lifespan. *PLOS Genet.* **9**, e1003214 (2013). [doi:10.1371/journal.pgen.1003214](https://doi.org/10.1371/journal.pgen.1003214) [Medline](#)
53. A. Y. Maslov, S. Ganapathi, M. Westerhof, W. Quispe-Tintaya, R. R. White, B. Van Houten, E. Reiling, M. E. T. Dollé, H. van Steeg, P. Hasty, J. H. J. Hoeijmakers, J. Vijg, DNA damage in normally and prematurely aged mice. *Aging Cell* **12**, 467–477 (2013). [doi:10.1111/acel.12071](https://doi.org/10.1111/acel.12071) [Medline](#)
54. M. L. Hamilton, H. Van Remmen, J. A. Drake, H. Yang, Z. M. Guo, K. Kewitt, C. A. Walter, A. Richardson, Does oxidative damage to DNA increase with age? *Proc. Natl. Acad. Sci. U.S.A.* **98**, 10469–10474 (2001). [doi:10.1073/pnas.171202698](https://doi.org/10.1073/pnas.171202698) [Medline](#)
55. R. E. Marioni, S. Shah, A. F. McRae, B. H. Chen, E. Colicino, S. E. Harris, J. Gibson, A. K. Henders, P. Redmond, S. R. Cox, A. Pattie, J. Corley, L. Murphy, N. G. Martin, G. W. Montgomery, A. P. Feinberg, M. D. Fallin, M. L. Multhaup, A. E. Jaffe, R. Joehanes, J. Schwartz, A. C. Just, K. L. Lunetta, J. M. Murabito, J. M. Starr, S. Horvath, A. A. Baccarelli, D. Levy, P. M. Visscher, N. R. Wray, I. J. Deary, DNA methylation age of blood predicts all-cause mortality in later life. *Genome Biol.* **16**, 25 (2015). [doi:10.1186/s13059-015-0584-6](https://doi.org/10.1186/s13059-015-0584-6) [Medline](#)
56. E. M. Michalak, M. L. Burr, A. J. Bannister, M. A. Dawson, The roles of DNA, RNA and histone methylation in ageing and cancer. *Nat. Rev. Mol. Cell Biol.* **20**, 573–589 (2019). [doi:10.1038/s41580-019-0143-1](https://doi.org/10.1038/s41580-019-0143-1) [Medline](#)
57. L. Bettledi, L. C. Foukas, Growth factor, energy and nutrient sensing signalling pathways in metabolic ageing. *Biogerontology* **18**, 913–929 (2017). [doi:10.1007/s10522-017-9724-6](https://doi.org/10.1007/s10522-017-9724-6) [Medline](#)
58. A. Bitto, T. K. Ito, V. V. Pineda, N. J. LeTexier, H. Z. Huang, E. Sutlief, H. Tung, N. Vizzini, B. Chen, K. Smith, D. Meza, M. Yajima, R. P. Beyer, K. F. Kerr, D. J. Davis, C. H. Gillespie, J. M. Snyder, P. M. Treuting, M. Kaeberlein, Transient rapamycin treatment can increase lifespan and healthspan in middle-aged mice. *eLife* **5**, e16351 (2016). [doi:10.7554/eLife.16351](https://doi.org/10.7554/eLife.16351) [Medline](#)
59. L. Ferrucci, E. Fabbri, Inflammageing: Chronic inflammation in ageing, cardiovascular disease, and frailty. *Nat. Rev. Cardiol.* **15**, 505–522 (2018). [doi:10.1038/s41569-018-0064-2](https://doi.org/10.1038/s41569-018-0064-2) [Medline](#)
60. J. Oh, Y. D. Lee, A. J. Wagers, Stem cell aging: Mechanisms, regulators and therapeutic opportunities. *Nat. Med.* **20**, 870–880 (2014). [doi:10.1038/nm.3651](https://doi.org/10.1038/nm.3651) [Medline](#)

61. N. Barker, J. H. van Es, J. Kuipers, P. Kujala, M. van den Born, M. Cozijnsen, A. Haegebarth, J. Korving, H. Begthel, P. J. Peters, H. Clevers, Identification of stem cells in small intestine and colon by marker gene *Lgr5*. *Nature* **449**, 1003–1007 (2007). [doi:10.1038/nature06196](https://doi.org/10.1038/nature06196) [Medline](#)
62. T. E. S. Kauppila, J. H. K. Kauppila, N. G. Larsson, Mammalian mitochondria and aging: An update. *Cell Metab.* **25**, 57–71 (2017). [doi:10.1016/j.cmet.2016.09.017](https://doi.org/10.1016/j.cmet.2016.09.017) [Medline](#)
63. J. Lin, P.-H. Wu, P. T. Tarr, K. S. Lindenberg, J. St-Pierre, C. Y. Zhang, V. K. Mootha, S. Jäger, C. R. Vianna, R. M. Reznick, L. Cui, M. Manieri, M. X. Donovan, Z. Wu, M. P. Cooper, M. C. Fan, L. M. Rohas, A. M. Zavacki, S. Cinti, G. I. Shulman, B. B. Lowell, D. Krainc, B. M. Spiegelman, Defects in adaptive energy metabolism with CNS-linked hyperactivity in *PGC-1α* null mice. *Cell* **119**, 121–135 (2004). [doi:10.1016/j.cell.2004.09.013](https://doi.org/10.1016/j.cell.2004.09.013) [Medline](#)
64. T. Suzuki, T. Suzuki, T. Wada, K. Saigo, K. Watanabe, Taurine as a constituent of mitochondrial tRNAs: New insights into the functions of taurine and human mitochondrial diseases. *EMBO J.* **21**, 6581–6589 (2002). [doi:10.1093/emboj/cdf656](https://doi.org/10.1093/emboj/cdf656) [Medline](#)
65. J. T. Pierce-Shimomura, B. L. Chen, J. J. Mun, R. Ho, R. Sarkis, S. L. McIntire, Genetic analysis of crawling and swimming locomotory patterns in *C. elegans*. *Proc. Natl. Acad. Sci. U.S.A.* **105**, 20982–20987 (2008). [doi:10.1073/pnas.0810359105](https://doi.org/10.1073/pnas.0810359105) [Medline](#)
66. M. Pietzner, I. D. Stewart, J. Raffler, K.-T. Khaw, G. A. Michelotti, G. Kastenmüller, N. J. Wareham, C. Langenberg, Plasma metabolites to profile pathways in noncommunicable disease multimorbidity. *Nat. Med.* **27**, 471–479 (2021). [doi:10.1038/s41591-021-01266-0](https://doi.org/10.1038/s41591-021-01266-0) [Medline](#)
67. D. E. Warburton, C. W. Nicol, S. S. Bredin, Prescribing exercise as preventive therapy. *CMAJ* **174**, 961–974 (2006). [doi:10.1503/cmaj.1040750](https://doi.org/10.1503/cmaj.1040750) [Medline](#)
68. B. K. Pedersen, B. Saltin, Exercise as medicine—Evidence for prescribing exercise as therapy in 26 different chronic diseases. *Scand. J. Med. Sci. Sports* **25**, 1–72 (2015). [doi:10.1111/sms.12581](https://doi.org/10.1111/sms.12581) [Medline](#)
69. J. Bergström, P. Fürst, L. O. Norée, E. Vinnars, Intracellular free amino acid concentration in human muscle tissue. *J. Appl. Physiol.* **36**, 693–697 (1974). [doi:10.1152/jappl.1974.36.6.693](https://doi.org/10.1152/jappl.1974.36.6.693) [Medline](#)
70. C. E. Wright, H. H. Tallan, Y. Y. Lin, G. E. Gaull, Taurine: Biological update. *Annu. Rev. Biochem.* **55**, 427–453 (1986). [doi:10.1146/annurev.bi.55.070186.002235](https://doi.org/10.1146/annurev.bi.55.070186.002235) [Medline](#)
71. I. H. Lambert, Regulation of the cellular content of the organic osmolyte taurine in mammalian cells. *Neurochem. Res.* **29**, 27–63 (2004). [doi:10.1023/B:NERE.0000010433.08577.96](https://doi.org/10.1023/B:NERE.0000010433.08577.96) [Medline](#)
72. I. Holopainen, P. Kontro, Taurine and hypotaurine transport by a single system in cultured neuroblastoma cells. *Acta Physiol. Scand.* **122**, 381–386 (1984). [doi:10.1111/j.1748-1716.1984.tb07522.x](https://doi.org/10.1111/j.1748-1716.1984.tb07522.x) [Medline](#)
73. K. Takahashi, M. Azuma, T. Yamada, Y. Ohyabu, K. Takahashi, S. W. Schaffer, J. Azuma, Taurine transporter in primary cultured neonatal rat heart cells: A comparison between

- cardiac myocytes and nonmyocytes. *Biochem. Pharmacol.* **65**, 1181–1187 (2003).
[doi:10.1016/S0006-2952\(03\)00003-0](https://doi.org/10.1016/S0006-2952(03)00003-0) Medline
74. S. S. Oja, I. Lehtinen, P. Lähdesmäki, Taurine transport rates between plasma and tissues in adult and 7-day-old mice. *Q. J. Exp. Physiol. Cogn. Med. Sci.* **61**, 133–143 (1976).
[doi:10.1113/expphysiol.1976.sp002344](https://doi.org/10.1113/expphysiol.1976.sp002344) Medline
75. G. Lee, H. Lee, J. Hong, S. H. Lee, B. H. Jung, Quantitative profiling of bile acids in rat bile using ultrahigh-performance liquid chromatography-orbitrap mass spectrometry: Alteration of the bile acid composition with aging. *J. Chromatogr. B Analyt. Technol. Biomed. Life Sci.* **1031**, 37–49 (2016). [doi:10.1016/j.jchromb.2016.07.017](https://doi.org/10.1016/j.jchromb.2016.07.017) Medline
76. R. Calvani, E. Brasili, G. Praticò, G. Capuani, A. Tomassini, F. Marini, F. Sciubba, A. Finamore, M. Roselli, E. Marzetti, A. Miccheli, Fecal and urinary NMR-based metabolomics unveil an aging signature in mice. *Exp. Gerontol.* **49**, 5–11 (2014).
[doi:10.1016/j.exger.2013.10.010](https://doi.org/10.1016/j.exger.2013.10.010) Medline
77. M. Barua, Y. Liu, M. R. Quinn, Taurine chloramine inhibits inducible nitric oxide synthase and TNF-alpha gene expression in activated alveolar macrophages: Decreased NF-κB activation and IkB kinase activity. *J. Immunol.* **167**, 2275–2281 (2001).
[doi:10.4049/jimmunol.167.4.2275](https://doi.org/10.4049/jimmunol.167.4.2275) Medline
78. J. J. DiNicolantonio, J. H. OKeefe, M. F. McCarty, Boosting endogenous production of vasoprotective hydrogen sulfide via supplementation with taurine and *N*-acetylcysteine: A novel way to promote cardiovascular health. *Open Heart* **4**, e000600 (2017).
[doi:10.1136/openhrt-2017-000600](https://doi.org/10.1136/openhrt-2017-000600) Medline
79. X. Shi, D. Yao, C. Chen, Identification of *N*-acetyltaurine as a novel metabolite of ethanol through metabolomics-guided biochemical analysis. *J. Biol. Chem.* **287**, 6336–6349 (2012). [doi:10.1074/jbc.M111.312199](https://doi.org/10.1074/jbc.M111.312199) Medline
80. T. Ito, S. Oishi, M. Takai, Y. Kimura, Y. Uozumi, Y. Fujio, S. W. Schaffer, J. Azuma, Cardiac and skeletal muscle abnormality in taurine transporter-knockout mice. *J. Biomed. Sci.* **17**, S20 (2010). [doi:10.1186/1423-0127-17-S1-S20](https://doi.org/10.1186/1423-0127-17-S1-S20) Medline
81. P. Roman-Garcia, I. Quiros-Gonzalez, L. Mottram, L. Lieben, K. Sharan, A. Wangwiwatsin, J. Tubio, K. Lewis, D. Wilkinson, B. Santhanam, N. Sarper, S. Clare, G. S. Vassiliou, V. R. Velagapudi, G. Dougan, V. K. Yadav, Vitamin B₁₂-dependent taurine synthesis regulates growth and bone mass. *J. Clin. Invest.* **124**, 2988–3002 (2014).
[doi:10.1172/JCI72606](https://doi.org/10.1172/JCI72606) Medline
82. J. P. de Magalhães, G. M. Church, Genomes optimize reproduction: Aging as a consequence of the developmental program. *Physiology* **20**, 252–259 (2005).
[doi:10.1152/physiol.00010.2005](https://doi.org/10.1152/physiol.00010.2005) Medline
83. A. V. Shindyapina, Y. Cho, A. Kaya, A. Tyshkovskiy, J. P. Castro, J. Gordevicius, J. R. Paganik, S. Horvath, L. Peshkin, V. N. Gladyshev, Rapamycin treatment during development extends lifespan and healthspan. bioRxiv 2022.2002.2018.481092 [Preprint] (2022); <https://doi.org/10.1101/2022.02.18.481092>.
84. M. Ansar, E. Ranza, M. Shetty, S. A. Paracha, M. Azam, I. Kern, J. Iwaszkiewicz, O. Farooq, C. J. Pournaras, A. Malcles, M. Kecik, C. Rivolta, W. Muzaffar, A. Qurban, L. Ali, Y. Aggoun, F. A. Santoni, P. Makrythanasis, J. Ahmed, R. Qamar, M. T. Sarwar, L. K. Henry, S. E. Antonarakis, Taurine treatment of retinal degeneration and

cardiomyopathy in a consanguineous family with SLC6A6 taurine transporter deficiency. *Hum. Mol. Genet.* **29**, 618–623 (2020). [doi:10.1093/hmg/ddz303](https://doi.org/10.1093/hmg/ddz303) Medline

85. L. Guan, P. Miao, The effects of taurine supplementation on obesity, blood pressure and lipid profile: A meta-analysis of randomized controlled trials. *Eur. J. Pharmacol.* **885**, 173533 (2020). [doi:10.1016/j.ejphar.2020.173533](https://doi.org/10.1016/j.ejphar.2020.173533) Medline
86. A. M. Brennan, M. Benson, J. Morningstar, M. Herzig, J. Robbins, R. E. Gerszten, R. Ross, Plasma metabolite profiles in response to chronic exercise. *Med. Sci. Sports Exerc.* **50**, 1480–1486 (2018). [doi:10.1249/MSS.0000000000001594](https://doi.org/10.1249/MSS.0000000000001594) Medline
87. C. Cuisinier, J. Michotte De Welle, R. K. Verbeeck, J. R. Poortmans, R. Ward, X. Sturbois, M. Francaux, Role of taurine in osmoregulation during endurance exercise. *Eur. J. Appl. Physiol.* **87**, 489–495 (2002). [doi:10.1007/s00421-002-0679-0](https://doi.org/10.1007/s00421-002-0679-0) Medline
88. S. Mangiola, P. Singh, K. Gollapalli, V.K. Yadav, Transcriptome changes in taurine deficient cells. Zenodo (2023); <https://doi.org/10.5281/zenodo.770045>.
89. K. Sharan, K. Lewis, T. Furukawa, V. K. Yadav, Regulation of bone mass through pineal-derived melatonin-MT2 receptor pathway. *J. Pineal Res.* **63**, e12423 (2017). [doi:10.1111/jpi.12423](https://doi.org/10.1111/jpi.12423) Medline
90. P. Singh, S. Telnova, B. Zhou, A. D. Mohamed, V. Mello, H. Wackerhage, X. E. Guo, A. K. Panda, V. K. Yadav, Maternal vitamin B₁₂ in mice positively regulates bone, but not muscle mass and strength in post-weaning and mature offspring. *Am. J. Physiol. Regul. Integr. Comp. Physiol.* **320**, R984–R993 (2021). [doi:10.1152/ajpregu.00355.2020](https://doi.org/10.1152/ajpregu.00355.2020) Medline
91. V. K. Yadav, G. Lakshmi, R. Medhamurthy, Prostaglandin F_{2α}-mediated activation of apoptotic signaling cascades in the corpus luteum during apoptosis: Involvement of caspase-activated DNase. *J. Biol. Chem.* **280**, 10357–10367 (2005). [doi:10.1074/jbc.M409596200](https://doi.org/10.1074/jbc.M409596200) Medline
92. M. B. Lee, D. T. Carr, M. G. Kiflezghi, Y. T. Zhao, D. B. Kim, S. Thon, M. D. Moore, M. A. K. Li, M. Kaeberlein, A system to identify inhibitors of mTOR signaling using high-resolution growth analysis in *Saccharomyces cerevisiae*. *Geroscience* **39**, 419–428 (2017). [doi:10.1007/s11357-017-9988-4](https://doi.org/10.1007/s11357-017-9988-4) Medline
93. K. K. Steffen, B. K. Kennedy, M. Kaeberlein, Measuring replicative life span in the budding yeast. *J. Vis. Exp.* **2009**, 1209 (2009). [doi:10.3791/1209-v](https://doi.org/10.3791/1209-v) Medline
94. C. Beaupere, L. Dinatto, B. M. Wasko, R. B. Chen, L. VanValkenburg, M. G. Kiflezghi, M. B. Lee, D. E. L. Promislow, W. Dang, M. Kaeberlein, V. M. Labunskyy, Genetic screen identifies adaptive aneuploidy as a key mediator of ER stress resistance in yeast. *Proc. Natl. Acad. Sci. U.S.A.* **115**, 9586–9591 (2018). [doi:10.1073/pnas.1804264115](https://doi.org/10.1073/pnas.1804264115) Medline
95. C. J. Murakami, V. Wall, N. Basisty, M. Kaeberlein, Composition and acidification of the culture medium influences chronological aging similarly in vineyard and laboratory yeast. *PLOS ONE* **6**, e24530 (2011). [doi:10.1371/journal.pone.0024530](https://doi.org/10.1371/journal.pone.0024530) Medline
96. M. B. Lee, M. G. Kiflezghi, M. Tsuchiya, B. Wasko, D. T. Carr, P. A. Uppal, K. A. Grayden, Y. C. Elala, T. A. Nguyen, J. Wang, P. Ragosti, S. Nguyen, Y. T. Zhao, D. Kim, S. Thon, I. Sinha, T. T. Tang, N. H. B. Tran, T. H. B. Tran, M. D. Moore, M. A. K. Li, K. Rodriguez, D. E. L. Promislow, M. Kaeberlein, *Pterocarpus marsupium* extract extends

- replicative lifespan in budding yeast. *Geroscience* **43**, 2595–2609 (2021). [doi:10.1007/s11357-021-00418-x](https://doi.org/10.1007/s11357-021-00418-x) [Medline](#)
97. B. Olsen, C. J. Murakami, M. Kaeberlein, YODA: Software to facilitate high-throughput analysis of chronological life span, growth rate, and survival in budding yeast. *BMC Bioinformatics* **11**, 141 (2010). [doi:10.1186/1471-2105-11-141](https://doi.org/10.1186/1471-2105-11-141) [Medline](#)
98. A. Aartsma-Rus, M. van Putten, Assessing functional performance in the *Mdx* mouse model. *J. Vis. Exp.* **2014**, 51303 (2014). [doi:10.3791/51303](https://doi.org/10.3791/51303) [Medline](#)
99. J. J. Chen, Z. Li, H. Pan, D. L. Murphy, H. Tamir, H. Koepsell, M. D. Gershon, Maintenance of serotonin in the intestinal mucosa and ganglia of mice that lack the high-affinity serotonin transporter: Abnormal intestinal motility and the expression of cation transporters. *J. Neurosci.* **21**, 6348–6361 (2001). [doi:10.1523/JNEUROSCI.21-16-06348.2001](https://doi.org/10.1523/JNEUROSCI.21-16-06348.2001) [Medline](#)
100. A. J. Mayorga, I. Lucki, Limitations on the use of the C57BL/6 mouse in the tail suspension test. *Psychopharmacology* **155**, 110–112 (2001). [doi:10.1007/s002130100687](https://doi.org/10.1007/s002130100687) [Medline](#)
101. C. M. Oh, J. Namkung, Y. Go, K. E. Shong, K. Kim, H. Kim, B.-Y. Park, H. W. Lee, Y. H. Jeon, J. Song, M. Shong, V. K. Yadav, G. Karsenty, S. Kajimura, I.-K. Lee, S. Park, H. Kim, Regulation of systemic energy homeostasis by serotonin in adipose tissues. *Nat. Commun.* **6**, 6794 (2015). [doi:10.1038/ncomms7794](https://doi.org/10.1038/ncomms7794) [Medline](#)
102. A. M. Parfitt, M. K. Drezner, F. H. Glorieux, J. A. Kanis, H. Malluche, P. J. Meunier, S. M. Ott, R. R. Recker, Bone histomorphometry: Standardization of nomenclature, symbols, and units. Report of the ASBMR Histomorphometry Nomenclature Committee. *J. Bone Miner. Res.* **2**, 595–610 (1987). [doi:10.1002/jbmr.5650020617](https://doi.org/10.1002/jbmr.5650020617) [Medline](#)
103. K. E. Lewis, K. Sharan, T. Takumi, V. K. Yadav, Skeletal site-specific changes in bone mass in a genetic mouse model for human 15q11-13 duplication seen in autism. *Sci. Rep.* **7**, 9902 (2017). [doi:10.1038/s41598-017-09921-8](https://doi.org/10.1038/s41598-017-09921-8) [Medline](#)
104. T. Hildebrand, A. Laib, R. Müller, J. Dequeker, P. Rüegsegger, Direct three-dimensional morphometric analysis of human cancellous bone: Microstructural data from spine, femur, iliac crest, and calcaneus. *J. Bone Miner. Res.* **14**, 1167–1174 (1999). [doi:10.1359/jbmr.1999.14.7.1167](https://doi.org/10.1359/jbmr.1999.14.7.1167) [Medline](#)
105. L. A. Feldkamp, S. A. Goldstein, A. M. Parfitt, G. Jesion, M. Kleerekoper, The direct examination of three-dimensional bone architecture in vitro by computed tomography. *J. Bone Miner. Res.* **4**, 3–11 (1989). [doi:10.1002/jbmr.5650040103](https://doi.org/10.1002/jbmr.5650040103) [Medline](#)
106. H. J. Gundersen, R. W. Boyce, J. R. Nyengaard, A. Odgaard, The Conneular: Unbiased estimation of connectivity using physical disectors under projection. *Bone* **14**, 217–222 (1993). [doi:10.1016/8756-3282\(93\)90144-Y](https://doi.org/10.1016/8756-3282(93)90144-Y) [Medline](#)
107. F. Debacq-Chainiaux, J. D. Erusalimsky, J. Campisi, O. Toussaint, Protocols to detect senescence-associated beta-galactosidase (SA- β gal) activity, a biomarker of senescent cells in culture and in vivo. *Nat. Protoc.* **4**, 1798–1806 (2009). [doi:10.1038/nprot.2009.191](https://doi.org/10.1038/nprot.2009.191) [Medline](#)
108. Y. Zhang, C. Park, C. Bennett, M. Thornton, D. Kim, Rapid and accurate alignment of nucleotide conversion sequencing reads with HISAT-3N. *Genome Res.* **31**, 1290–1295 (2021). [doi:10.1101/gr.275193.120](https://doi.org/10.1101/gr.275193.120) [Medline](#)

109. G. H. Putri, S. Anders, P. T. Pyl, J. E. Pimanda, F. Zanini, Analysing high-throughput sequencing data in Python with HTSeq 2.0. *Bioinformatics* **38**, 2943–2945 (2022). [doi:10.1093/bioinformatics/btac166](https://doi.org/10.1093/bioinformatics/btac166) [Medline](#)
110. H. Wickham, M. Averick, J. Bryan, W. Chang, L. McGowan, R. François, G. Grolemund, A. Hayes, L. Henry, J. Hester, M. Kuhn, T. Pedersen, E. Miller, S. Bache, K. Müller, J. Ooms, D. Robinson, D. Seidel, V. Spinu, K. Takahashi, D. Vaughan, C. Wilke, K. Woo, H. Yutani, Welcome to the Tidyverse. *J. Open Source Softw.* **4**, 1686 (2019). [doi:10.21105/joss.01686](https://doi.org/10.21105/joss.01686)
111. M. D. Robinson, D. J. McCarthy, G. K. Smyth, edgeR: A Bioconductor package for differential expression analysis of digital gene expression data. *Bioinformatics* **26**, 139–140 (2010). [doi:10.1093/bioinformatics/btp616](https://doi.org/10.1093/bioinformatics/btp616) [Medline](#)
112. M. D. Robinson, A. Oshlack, A scaling normalization method for differential expression analysis of RNA-seq data. *Genome Biol.* **11**, R25 (2010). [doi:10.1186/gb-2010-11-3-r25](https://doi.org/10.1186/gb-2010-11-3-r25) [Medline](#)
113. X. Zhou, H. Lindsay, M. D. Robinson, Robustly detecting differential expression in RNA sequencing data using observation weights. *Nucleic Acids Res.* **42**, e91 (2014). [doi:10.1093/nar/gku310](https://doi.org/10.1093/nar/gku310) [Medline](#)
114. D. J. McCarthy, G. K. Smyth, Testing significance relative to a fold-change threshold is a TREAT. *Bioinformatics* **25**, 765–771 (2009). [doi:10.1093/bioinformatics/btp053](https://doi.org/10.1093/bioinformatics/btp053) [Medline](#)
115. S. Mangiola, E. A. Thomas, M. Modrák, A. Vehtari, A. T. Papenfuss, Probabilistic outlier identification for RNA sequencing generalized linear models. *NAR Genom. Bioinform.* **3**, lqab005 (2021). [doi:10.1093/nargab/lqab005](https://doi.org/10.1093/nargab/lqab005) [Medline](#)
116. H. Wickham, *ggplot2: Elegant Graphics for Data Analysis* (Springer, 2016).
117. S. P. Mangiola, A. T. Papenfuss, tidyHeatmap: An R package for modular heatmap production based on tidy principles. *J. Open Source Softw.* **5**, 2472 (2020). [doi:10.21105/joss.02472](https://doi.org/10.21105/joss.02472)
118. Z. Gu, R. Eils, M. Schlesner, Complex heatmaps reveal patterns and correlations in multidimensional genomic data. *Bioinformatics* **32**, 2847–2849 (2016). [doi:10.1093/bioinformatics/btw313](https://doi.org/10.1093/bioinformatics/btw313) [Medline](#)
119. G. Yu, L. G. Wang, Y. Han, Q. Y. He, clusterProfiler: An R package for comparing biological themes among gene clusters. *OMICS* **16**, 284–287 (2012). [doi:10.1089/omi.2011.0118](https://doi.org/10.1089/omi.2011.0118) [Medline](#)
120. A. Hernandez-Segura, T. V. de Jong, S. Melov, V. Guryev, J. Campisi, M. Demaria, Unmasking transcriptional heterogeneity in senescent cells. *Curr. Biol.* **27**, 2652–2660.e4 (2017). [doi:10.1016/j.cub.2017.07.033](https://doi.org/10.1016/j.cub.2017.07.033) [Medline](#)
121. Y. Hochberg, Y. Benjamini, More powerful procedures for multiple significance testing. *Stat. Med.* **9**, 811–818 (1990). [doi:10.1002/sim.4780090710](https://doi.org/10.1002/sim.4780090710) [Medline](#)
122. S. Verlaan, T. J. Aspray, J. M. Bauer, T. Cederholm, J. Hemsworth, T. R. Hill, J. S. McPhee, M. Piasecki, C. Seal, C. C. Sieber, S. Ter Borg, S. L. Wijers, K. Brandt, Nutritional status, body composition, and quality of life in community-dwelling sarcopenic and non-sarcopenic older adults: A case-control study. *Clin. Nutr.* **36**, 267–274 (2017). [doi:10.1016/j.clnu.2015.11.013](https://doi.org/10.1016/j.clnu.2015.11.013) [Medline](#)

123. S. Rausser, C. Trumpf, M. A. McGill, A. Junker, W. Wang, S.-H. Ho, A. Mitchell, K. R. Karan, C. Monk, S. C. Segerstrom, R. G. Reed, M. Picard, Mitochondrial phenotypes in purified human immune cell subtypes and cell mixtures. *eLife* **10**, e70899 (2021). [doi:10.7554/eLife.70899](https://doi.org/10.7554/eLife.70899) [Medline](#)
124. N. Anand, A. Holcom, M. Broussalian, M. Schmidt, S. J. Chinta, G. J. Lithgow, J. K. Andersen, M. Chamoli, Dysregulated iron metabolism in *C. elegans* catp-6/ATP13A2 mutant impairs mitochondrial function. *Neurobiol. Dis.* **139**, 104786 (2020). [doi:10.1016/j.nbd.2020.104786](https://doi.org/10.1016/j.nbd.2020.104786) [Medline](#)
125. M. Vanharanta, S. Voutilainen, T. H. Rissanen, H. Adlercreutz, J. T. Salonen, Risk of cardiovascular disease-related and all-cause death according to serum concentrations of enterolactone: Kuopio Ischaemic Heart Disease Risk Factor Study. *Arch. Intern. Med.* **163**, 1099–1104 (2003). [doi:10.1001/archinte.163.9.1099](https://doi.org/10.1001/archinte.163.9.1099) [Medline](#)
126. K. L. Kolho, A. Pessia, T. Jaakkola, W. M. de Vos, V. Velagapudi, Faecal and serum metabolomics in paediatric inflammatory bowel disease. *J. Crohn's Colitis* **11**, 321–334 (2017). [Medline](#)
127. J. Buzkova, J. Nikkanen, S. Ahola, A. H. Hakonen, K. Sevastianova, T. Hovinen, H. Yki-Järvinen, K. H. Pietiläinen, T. Lönnqvist, V. Velagapudi, C. J. Carroll, A. Suomalainen, Metabolomes of mitochondrial diseases and inclusion body myositis patients: Treatment targets and biomarkers. *EMBO Mol. Med.* **10**, e9091 (2018). [doi:10.15252/emmm.201809091](https://doi.org/10.15252/emmm.201809091) [Medline](#)
128. N. Day, S. Oakes, R. Luben, K. T. Khaw, S. Bingham, A. Welch, N. Wareham, EPIC-Norfolk: Study design and characteristics of the cohort. European Prospective Investigation of Cancer. *Br. J. Cancer* **80**, 95–103 (1999). [Medline](#)
129. D. Schranner, M. Schönfelder, W. Römisch-Margl, J. Scherr, J. Schlegel, O. Zelger, A. Riermeier, S. Kaps, C. Prehn, J. Adamski, Q. Söhnlein, F. Stöcker, F. Kreuzpointner, M. Halle, G. Kastenmüller, H. Wackerhage, Physiological extremes of the human blood metabolome: A metabolomics analysis of highly glycolytic, oxidative, and anabolic athletes. *Physiol. Rep.* **9**, e14885 (2021). [doi:10.14814/phy2.14885](https://doi.org/10.14814/phy2.14885) [Medline](#)
130. N. Percie du Sert, V. Hurst, A. Ahluwalia, S. Alam, M. T. Avey, M. Baker, W. J. Browne, A. Clark, I. C. Cuthill, U. Dirnagl, M. Emerson, P. Garner, S. T. Holgate, D. W. Howells, N. A. Karp, S. E. Lazic, K. Lidster, C. J. MacCallum, M. Macleod, E. J. Pearl, O. H. Petersen, F. Rawle, P. Reynolds, K. Rooney, E. S. Sena, S. D. Silberberg, T. Steckler, H. Würbel, The ARRIVE guidelines 2.0: Updated guidelines for reporting animal research. *Br. J. Pharmacol.* **177**, 3617–3624 (2020). [doi:10.1111/bph.15193](https://doi.org/10.1111/bph.15193) [Medline](#)